TKK Dissertations 123
Espoo 2008

AN ADAPTIVE OBSERVER WITH SIGNAL INJECTION FOR INTERIOR PERMANENT MAGNET SYNCHRONOUS MOTORS

Doctoral Dissertation

Antti Piippo

Helsinki University of Technology
Faculty of Electronics, Communications and Automation
Department of Electrical Engineering

TKK Dissertations 123
Espoo 2008

AN ADAPTIVE OBSERVER WITH SIGNAL INJECTION FOR INTERIOR PERMANENT MAGNET SYNCHRONOUS MOTORS

Doctoral Dissertation

Antti Piippo

Dissertation for the degree of Doctor of Science in Technology to be presented with due permission of the Faculty of Electronics, Communications and Automation for public examination and debate in Auditorium S4 at Helsinki University of Technology (Espoo, Finland) on the 30th of May, 2008, at 12 noon.

Helsinki University of Technology
Faculty of Electronics, Communications and Automation
Department of Electrical Engineering

Teknillinen korkeakoulu
Elektroniikan, tietoliikenteen ja automaation tiedekunta
Sähkötekniikan laitos

Distribution:
Helsinki University of Technology
Faculty of Electronics, Communications and Automation
Department of Electrical Engineering
P.O. Box 3000
FI - 02015 TKK
FINLAND
URL: http://powerelectronics.tkk.fi/
Tel. +358-9-451 2431
Fax +358-9-451 2432
E-mail: antti.piippo@fi.abb.com

ISBN 978-951-22-9378-0
ISBN 978-951-22-9379-7 (PDF)
ISSN 1795-2239
ISSN 1795-4584 (PDF)
URL: http://lib.tkk.fi/Diss/2008/isbn9789512293797/

TKK-DISS-2472

Multiprint Oy
Espoo 2008

ABSTRACT OF DOCTORAL DISSERTATION	HELSINKI UNIVERSITY OF TECHNOLOGY P. O. BOX 1000, FI-02015 TKK http://www.tkk.fi

Author Antti Piippo

Name of the dissertation

An Adaptive Observer With Signal Injection for Interior Permanent Magnet Synchronous Motors

Manuscript submitted 12.11.2007	Manuscript revised 01.04.2008
Date of the defence 30.05.2008	
☐ Monograph	☒ Article dissertation (summary + original articles)
Faculty	Faculty of Electronics, Communications and Automation
Department	Department of Electrical Engineering
Field of research	Electrical Engineering
Opponent(s)	Prof. Alfio Consoli
Supervisor	Prof. Jorma Luomi
Instructor	

Abstract

This thesis deals with methods for the sensorless control of permanent magnet synchronous motors. The methods are investigated by means of theoretical analysis, simulations, and laboratory experiments with a 2.2-kW interior-magnet motor. To expand the operating range and to improve the estimation dynamics, two hybrid speed and position estimation methods are proposed. In the methods, high-frequency signal injection is used for stabilizing a modified voltage model and an adaptive observer at low speeds. The hybrid methods allow sustained operation at low speeds, yet preserve good dynamic properties. For the adaptive observer, an observer gain is selected such that the estimation dynamics are improved. To reduce the sensitivity of the adaptive observer to the motor parameter errors, a method is developed where two electrical parameters are estimated on-line. A model for the spatial harmonics in the permanent magnet motors is included in the adaptive observer for the reduction of estimation errors, and the signal injection method is modified to improve position estimation accuracy when inductance harmonics are present. In addition, a method is proposed for suppressing the electromagnetic torque ripple caused by the spatial harmonics. A control system and a full-order observer are also developed for drives equipped with an LC filter at the inverter output. It is also shown that signal injection can be used with the filter if the injection frequency is suitably chosen. For drives equipped with DC-link current measurement, a method is proposed that also uses high-frequency signal injection at low speeds.

Keywords Permanent magnet synchronous motor, sensorless control, adaptive observer, signal injection	
ISBN (printed) 978-951-22-9378-0	ISSN (printed) 1795-2239
ISBN (pdf) 978-951-22-9379-7	ISSN (pdf) 1795-4584
Language English	Number of pages 163
Publisher Multiprint Oy	
Print distribution Department of Electrical Engineering	
☒ The dissertation can be read at http://lib.tkk.fi/Diss/2008/isbn9789512293797/	

VÄITÖSKIRJAN TIIVISTELMÄ	TEKNILLINEN KORKEAKOULU PL 1000, 02015 TKK http://www.tkk.fi

Tekijä Antti Piippo

Väitöskirjan nimi

Signaali-injektiolla täydennetty adaptiivinen havaitsija sisämagneettitahtimoottorille

Käsikirjoituksen päivämäärä 12.11.2007	Korjatun käsikirjoituksen päivämäärä 01.04.2008

Väitöstilaisuuden ajankohta 30.05.2008

☐ Monografia	☒ Yhdistelmäväitöskirja (yhteenveto + erillisartikkelit)

Tiedekunta	Elektroniikan, tietoliikenteen ja automaation tiedekunta
Laitos	Sähkötekniikan laitos
Tutkimusala	Sähkötekniikka
Vastaväittäjä(t)	Prof. Alfio Consoli
Työn valvoja	Prof. Jorma Luomi
Työn ohjaaja	

Tiivistelmä

Tämä väitöskirja käsittelee kestomagnetoidun tahtikoneen anturittomia ohjausmenetelmiä. Menetelmiä tutkitaan teoreettisen analyysin, simulointien ja 2,2 kW:n tehoisella kestomagneettitahtikoneella tehtyjen laboratoriokokeiden avulla. Toiminta-alueen laajentamiseksi ja dynamiikan parantamiseksi ehdotetaan kahta hybridimenetelmää nopeuden ja asennon estimoimiseksi. Menetelmissä suuritaajuista signaali-injektiota käytetään stabiloimaan muokattu jännitemalli ja adaptiivinen havaitsija pienillä nopeuksilla. Menetelmät mahdollistavat jatkuvan toiminnan pienillä nopeuksilla säilyttäen hyvät dynaamiset ominaisuudet. Adaptiivisen havaitsijan vahvistus valitaan siten, että estimoinnin dynamiikkaa saadaan parannettua. Adaptiivisen havaitsijan parametriherkkyyden pienentämiseksi kehitetään menetelmä kahden parametrin estimointiin. Adaptiiviseen havaitsijaan sisällytetään malli kestomagneettikoneen yliaalloille estimointivirheiden pienentämiseksi, ja signaali-injektiomenetelmää muokataan asennon estimoinnin tarkkuuden parantamiseksi, kun induktanssissa on yliaaltoja. Lisäksi ehdotetaan menetelmää kestomagneettikoneen yliaaltojen aiheuttaman vääntömomentin aaltoisuuden vaimentamiseksi. Säätöjärjestelmä ja täyden kertaluvun havaitsija kehitetään myös taajuusmuuttajan lähtösuodattimella varustetulle sähkökäytölle. Myös signaali-injektion osoitetaan toimivan lähtösuodattimen kanssa, jos injektion taajuus valitaan sopivasti. Taajuusmuuttajan välipiirivirran mittauksella varustettuja käyttöjä varten ehdotetaan menetelmää, jossa käytetään myös signaali-injektiota pienillä nopeuksilla.

Asiasanat Kestomagneettitahtikone, anturiton ohjaus, adaptiivinen havaitsija, signaali-injektio

ISBN (painettu) 978-951-22-9378-0	ISSN (painettu) 1795-2239
ISBN (pdf) 978-951-22-9379-7	ISSN (pdf) 1795-4584
Kieli Englanti	Sivumäärä 163

Julkaisija Multiprint Oy

Painetun väitöskirjan jakelu Sähkötekniikan laitos

☒ Luettavissa verkossa osoitteessa http://lib.tkk.fi/Diss/2008/isbn9789512293797/

Preface

Since the beginning of 2003, I have been working on the control of permanent magnet synchronous machines. After completing my Master's thesis on the topic, it was clear to me that I still wanted to address the challenges related to it. Since October 2003, I have been working on this thesis at Power Electronics Laboratory, Helsinki University of Technology. The work has been a part of a research project that deals with control of AC machines and is financed by ABB Oy. I have had a position at the Graduate School of Electrical Engineering from 2004 through 2007. I also gratefully acknowledge the financial support given by the Walter Ahlström Foundation and Kaupallisten ja teknillisten tieteiden tukisäätiö (KAUTE).

I owe my greatest gratitude to Prof. Jorma Luomi, the supervisor of this thesis. Due to his excellent guidance, I have learned a tremendous amount about academic work, and maybe most importantly, scientific writing. Prof. Luomi has also assured that the equipment for experimental research has been up to date and the funding for the research has been constant, allowing researchers to concentrate on their work. I wish to thank Dr. Marko Hinkkanen for his guidance and ideas. His points of view have often led my work in the correct direction. I would also like to thank the official pre-examiners of the thesis, Prof. Seung-Ki Sul and Prof. Heikki Tuusa. They presented valuable comments and constructive criticism that helped improve the manuscript.

I also owe my thanks to my other colleagues, Dr. Janne Salomäki, Dr. Petri Mäki-Ontto, Mr. Henri Kinnunen, and Mrs. Mikaela Ranta. All the staff of Power Electronics Laboratory have contributed to creating a friendly and pleasant atmosphere. I would also like to thank the head of the laboratory, Prof. Jorma Kyyrä, secretary, Mrs. Anja Meuronen, and laboratory technician, Mr. Ilkka Hanhivaara.

My appreciation goes to ABB Oy for financing the project. I am grateful to Mr. Matti Kauhanen and Mr. Mikko Korpinen, who have brought out important standpoints while organizing the project on behalf of ABB Oy. The ideas learnt from Mr. Mikko Vertanen, Mr. Samuli Heikkilä, Mr. Kalle Suomela, and Mr. Matti Mustonen have also been helpful.

Finally, I would like to thank my wife Mervi for her love and support during the work, and also our one-year-old son Miro for his personal way to relieve the author's stress.

Espoo, April 2008

Antti Piippo

Contents

List of Publications **11**

Symbols and Abbreviations **13**

1 Introduction **15**

2 System Model **19**
2.1 PMSM Drive Systems 19
2.2 PMSM Model With Spatial Harmonics 20
2.3 Magnetic Saturation 25
2.4 Inverter Output Filter Model 26

3 Sensorless Vector Control **27**
3.1 Fundamental-Excitation Methods 27
3.1.1 Modified Voltage Models 28
3.1.2 Adaptive Observers 30
3.2 Signal Injection Methods 33
3.3 Hybrid Methods 39
3.4 Effect of Parameter Errors and Parameter Adaptation 50
3.5 Cascaded Speed and Current Control 50
3.6 Torque Ripple Compensation 51
3.7 Sensorless Control With Inverter Output Filter 54
3.8 DC-link Current Measurement 56

4 Experimental Setup **59**

5 Summaries of Publications **63**
5.1 Abstracts 63
5.2 Contribution of the Thesis 65

6 Conclusions **67**

Bibliography **69**

List of Publications

This thesis consists of an overview and the following publications:

I Piippo, A., Hinkkanen, M., and Luomi, J. (2004). "Sensorless control of PMSM drives using a combination of voltage model and HF signal injection." In *Conference Record of the 39th IEEE-Industry Applications Society (IAS) Annual Meeting*, vol. 2, pp. 964–970, Seattle, WA.

II Piippo, A. and Luomi, J. (2005). "Adaptive observer combined with HF signal injection for sensorless control of PMSM drives." In *Proceedings of the IEEE International Electric Machines and Drives Conference (IEMDC'05)*, pp. 674–681, San Antonio, TX.

III Piippo, A., Hinkkanen, M., and Luomi, J. (2008). "Analysis of an adaptive observer for sensorless control of interior permanent magnet synchronous motors." *IEEE Transactions on Industrial Electronics*, **55**(2), pp. 570-576.

IV Piippo, A. and Luomi, J. (2006). "Inductance harmonics in permanent magnet synchronous motors and reduction of their effects in sensorless control." In *Proceedings of the XVII International Conference on Electric Machines (ICEM 2006)*, no. 138, Chania, Greece, CD-ROM.

V Piippo, A. and Luomi, J. (2006). "Torque ripple reduction in sensorless PMSM drives." In *Proceedings of The 32nd Annual Conference of the IEEE Industrial Electronics Society (IECON'06)*, pp. 920–925, Paris, France.

VI Salomäki, J., Piippo, A., Hinkkanen, M., and Luomi, J. (2006). "Sensorless vector control of PMSM drives equipped with inverter output filter." In *Proceedings of The 32nd Annual Conference of the IEEE Industrial Electronics Society (IECON'06)*, pp. 1059–1064, Paris, France.

VII Piippo, A., Salomäki, J., and Luomi, J. "Signal injection in sensorless PMSM drives equipped with inverter output filter." *IEEE Transactions on Industry Applications*. (In press)

VIII Piippo, A., Suomela, K., Hinkkanen, M., and Luomi, J. (2007). "Sensorless PMSM drive with DC-link current measurement." In *Conference Record of the 42nd IEEE-Industry Applications Society (IAS) Annual Meeting*, pp. 2371–2377, New Orleans, LA.

IX Piippo, A., Hinkkanen, M., and Luomi, J. "Adaptation of motor parameters in sensorless PMSM drives." *IEEE Transactions on Industry Applications*. (In press)

The author has written Publications **I**, **III**, **VIII**, and **IX** with the help and guidance of Prof. Jorma Luomi and Dr. Marko Hinkkanen, and Publications **II**, **IV**, **V**, and **VII** with help and guidance from Prof. Luomi. Dr. Janne Salomäki has mainly written Publication **VI**.

In Publications **VI** and **VII**, the author and Dr. Salomäki have been jointly responsible for the adaptive full-order observer. Dr. Salomäki has done the literature review and the cascade control system, whereas the author has modeled the permanent magnet motor. In Publication **VI**, Dr. Salomäki has performed the linearization analysis. The author is responsible for the high-frequency signal injection and the investigation of the effects of the filter on it in Publication **VII**. In Publication **IX**, the author is responsible for the parameter adaptation laws and the experiments, whereas Dr. Marko Hinkkanen has performed the quasi-steady-state and linearization analyses.

Preliminary versions of Publications **III**, **VII**, and **IX** were presented at conferences (Piippo et al., 2005), (Piippo et al., 2007b), (Piippo et al., 2007a).

Symbols and Abbreviations

Symbols

b	Viscous damping constant
C_f	Capacitance of inverter output filter
F_ε	Observer error
$\mathbf{I}$	Identity matrix
i_a, i_b, i_c	Phase currents
$\mathbf{i}_A$	Inverter output current vector in the rotor reference frame
i_{Ad}, i_{Aq}	d- and q-axis components of the inverter output current
$\mathbf{i}_s$	Stator current vector in the rotor reference frame
i_d, i_{sd}	Stator d-axis current component
i_q, i_{sq}	Stator q-axis current component
i_{dc}	DC-link current at the input of the inverter
$\mathbf{J}$	Orthogonal rotation matrix
J	Moment of inertia
$\mathbf{L}_s$	Stator inductance matrix
L_d	Stator d-axis inductance
L_{d0}	Unsaturated value of stator d-axis inductance
L_q	Stator q-axis inductance
L_{q0}	Unsaturated value of stator q-axis inductance
L_6	Stator inductance 6th harmonic in the rotor reference frame
L_f	Inductance of inverter output filter choke
k_i	Integral gain of the adaptation mechanism
k_p	Proportional gain of the adaptation mechanism
K_ε	Signal injection gain
p	Number of pole pairs
R_s	Stator resistance
R_{Lf}	Series resistance of inverter output filter choke
$\mathbf{T}$	Coordinate transformation matrix
T_e	Electromagnetic torque
T_N	Nominal torque
T_l	Load torque
u_a, u_b, u_c	Phase voltages
$\mathbf{u}_A$	Inverter output voltage vector in the rotor reference frame

u_{Ad}, u_{Aq}	d- and q-axis components of the inverter output voltage
$\hat{u}_c$	Amplitude of the signal injection voltage
u_{dc}	DC-link voltage at the input of the inverter
$\mathbf{u}_s$	Stator voltage vector in the rotor reference frame
u_d, u_{sd}	Stator d-axis voltage component
u_q, u_{sq}	Stator q-axis voltage component
α_{fo}	Bandwidth of the speed adaptation mechanism
α_i	Bandwidth of the PI mechanism
γ_i	Integral gain of the PI mechanism
γ_p	Proportional gain of the PI mechanism
ε	Error signal of the signal injection method
$\boldsymbol{\lambda}$	Observer gain
ω_c	Angular frequency of the signal injection voltage
ω_m	Electrical angular speed of the rotor
$\boldsymbol{\psi}_s$	Stator flux in the rotor reference frame
ψ_{pm}	Permanent magnet flux
ψ_{pm0}	Fundamental component of the permanent magnet flux
ψ_{d6}	6th harmonic of the permanent magnet flux on the d axis
ψ_{q6}	6th harmonic of the permanent magnet flux on the q axis
θ_m	Rotor position in electrical radians

Bold symbols denote matrix or vector quantities. Estimated quantities are marked by the symbol $\hat{}$ and estimation errors by $\tilde{}$. Quantities expressed in the stator reference frame are marked by the superscript s and measured quantities expressed in the estimated rotor reference frame by $'$. Reference quantities are represented by the subscript ref.

Abbreviations

AC	Alternating current
DC	Direct current
DTC	Direct torque control
HF	High frequency
IP	Integral-proportional
PI	Proportional-integral
PMSM	Permanent magnet synchronous motor
PWM	Pulse-width modulation
SVPWM	Space-vector pulse-width modulation

Chapter 1

Introduction

Electric drives are significant electricity consumers in industrialized countries. Adjusting the rotational speed of the motor enables more accurate process control and reduces energy consumption. Modern variable-speed drives consist of an alternating-current (AC) motor that is fed by a frequency converter. The induction motor is the most common motor type due to its rugged construction, negligible maintenance requirement, and low price.

Permanent magnet synchronous motors are today becoming common in electric drives. Compared to induction motors, the absence of the magnetizing current leads to reduced resistive losses in the stator. As the resistive losses in the rotor are also absent, the efficiency of the permanent magnet synchronous motor (PMSM) is higher than that of the induction motor. Hence, a motor of the same size can be rated to a higher power with the same losses. Torque-to-weight ratio is a frequently mentioned quantity when referring to the higher specific power of a PMSM.

The simplest way to control AC motors is the constant volts-per-hertz control, or scalar control. The more advanced control methods include stator current vector control (Blaschke, 1972) and hysteresis control of the estimated stator flux. The methods in the latter category are known as direct torque control (DTC) (Takahashi and Noguchi, 1986) or direct self control (Depenbrock, 1988). PMSMs are principally controlled by vector control or DTC, both of which provide the ability to control the electromagnetic torque produced by the motor. In vector control, the stator current is used to control the flux and the torque, whereas two-point control is used to control the stator flux and the torque in DTC. This thesis concentrates on vector control.

For vector control of permanent magnet motors, information on the rotor position is needed. The position is traditionally measured by a sensor mounted on the shaft of the motor. The bulky position sensor increases the cost of the drive, makes the installation more difficult, and needs additional wiring. The position sensor reduces the reliability of the drive since its failure causes a break in the operation. In worst cases, the process in which the drive is involved is also interrupted.

The rotor position can be estimated instead of measuring it. In these motion-sensorless methods, the rotor speed and position are estimated by using the known stator voltages and currents of the motor. Sensorless control has been under keen investigation in recent years, since the reliability of the motor drive is improved and the cost is decreased when the position sensor can be eliminated. Among the first sensorless methods for the PMSMs, Wu and Slemon (1991) estimated the stator flux using the phase voltage equations. This kind of an estimator, using the dynamic model of the stator winding for the flux estimation, is often referred to as a voltage model. More generally, methods based on the dynamic model

of the motor are known as fundamental-excitation methods. Another kind of approach for the rotor position estimation is to use a signal injection method, where spatial anisotropies in the machine are tracked by an excitation signal, which usually has a high frequency (Schroedl, 1996; Jansen and Lorenz, 1995).

Challenges in Sensorless Control

Fundamental-excitation methods have good dynamic properties, but they are based on a model of the motor. Since motor parameter estimates are needed in the motor model, the estimation is sensitive to errors in these parameters (Kim et al., 1995). The methods are based on the detection of the rotor-induced back-electromotive force (back-emf), which is proportional to the rotor speed. Thus, when the speed decreases, the significance of the parameter errors increases as the weakening back-emf has to be distinguished from the resistive voltage drop. The methods suffer from estimation errors and stability problems at low speeds even with sufficiently accurate parameter estimates, because noise and measurement errors are also present. At zero speed, the PMSM is unobservable by fundamental-excitation methods, and sustained operation is not possible in loaded conditions.

Signal injection methods, on the other hand, can detect the rotor position even at standstill. However, the injection of a high-frequency (HF) excitation signal causes additional losses and audible noise. The voltage required for HF excitation becomes a restriction at high rotor speeds. The methods are also sensitive to inverter nonlinearities (Jeong and Park, 1991) and magnetic saturation (Li et al., 2007), and they tend to have limited dynamic performance as compared to fundamental-excitation methods.

In PMSMs, the magnetomotive force distribution is not perfectly sinusoidal and neither is the spatial variation of the stator inductances (Low et al., 1990). Higher-order variations in the permanent magnet flux linkage and stator inductances, often referred to as spatial harmonics, disturb both the fundamental-excitation methods (De Angelo et al., 2005) and signal injection methods (Degner and Lorenz, 1998). As a result, substantial oscillations may occur in the rotor speed estimate, and the rotor position can have a periodic error. The spatial harmonics cause load-dependent torque ripple (Low et al., 1990) in addition to the cogging torque caused by the stator slotting.

In electric drives supplied by a pulsewidth-modulated inverter, the high-frequency components of the inverter output voltage cause undesired effects in the motor. These include additional losses, stresses in the winding insulations, and audible noise. An LC filter, added between the inverter and the motor, is a common solution to these problems (Carpita et al., 1991). However, the filter complicates the motor control. For the current control, the effects of the filter have to be compensated, and if sensorless control is used, the filter has to be taken into account in the estimation. The previously published estimation methods for PMSMs require measurements of the motor voltages and currents (Batzel and Lee, 2005), which differ from those of the inverter output due to the presence of the filter. Methods capable of low-speed operation without a motion sensor have so far not been available.

In low-cost frequency converters, a DC-link current measurement is often used instead of the phase current measurements, mainly due to the lower cost (Green and Williams, 1989). For vector control, the phase currents have to be estimated from the DC-link current. In some of the existing sensorless methods, modified pulse-width modulation (PWM)

patterns are used in order to estimate the phase currents (Habetler and Divan, 1991), which results in additional losses in the motor and audible noise. Another alternative is to use special current sampling (Blaabjerg et al., 1997), which makes the control software more complicated.

Objective and Outline of the Thesis

The objective of this thesis is to develop a robust, reliable, cost-effective, and high-performance sensorless vector control method for PMSM drives. In more detail, the objectives include the following:

- To create an estimator capable of wide-speed-range operation with good dynamic properties by combining a fundamental-excitation method and a signal injection method
- To improve the dynamics of the estimation
- To reduce the parameter sensitivity of fundamental-excitation methods by parameter adaptation
- To reduce the effects of the unidealities in the PMSM on the estimation
- To create a sensorless method for the electromagnetic torque ripple suppression
- To develop a sensorless method capable of low-speed operation with an inverter output filter
- To develop a method capable of operation in a wide speed range in PMSM drives equipped with an inverter DC-link current measurement

The thesis consists of this compendium and nine publications. The overview is outlined as follows. Chapter 2 defines the system including the permanent magnet motor. A model for the spatial harmonics of the PMSM is defined, and different systems used in combination with the motor are introduced. Chapter 3 discusses the sensorless control methods. The fundamental-excitation methods, the signal injection methods, and the combined observers are reviewed. The sensitivity of fundamental-excitation methods to the motor parameter errors is discussed, and a method for the parameter adaptation is introduced. A model for the spatial harmonics of the PMSM is added into the fundamental-excitation method, and the signal injection method is modified for better estimation accuracy at low speeds. The methods for reducing the torque ripple are reviewed, and sensorless control with an inverter output filter is discussed. Methods applicable to a drive with DC-link current measurement are also considered. The experimental setup used for the experimental research is described in Chapter 4. The summaries of the publications and the scientific contributions of the thesis are listed in Chapter 5, and Chapter 6 concludes the thesis.

Chapter 2

System Model

2.1 PMSM Drive Systems

In the variable-speed PMSM drive dealt with in this thesis, the PMSM is fed by a frequency converter having a voltage DC link. A block diagram of a variable-speed drive consisting of the PMSM and a frequency converter is shown in Fig. 2.1. The DC-link voltage u_{dc} and the inverter output current $\mathbf{i}_s$ are measured and used for feedback in the control algorithms. $\omega_{m,ref}$ is the electrical angular speed reference. This type of setup is used in Publications **I**-**V** and **IX**.

A block diagram of a system including an LC filter in the inverter output is shown in Fig. 2.2. The inverter output current $\mathbf{i}_A$ and the DC-link voltage u_{dc} are measured. A system with the LC filter is used in Publications **VI** and **VII**.

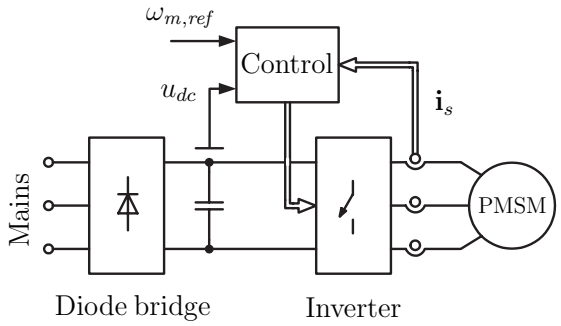

Figure 2.1: Motion-sensorless PMSM drive system.

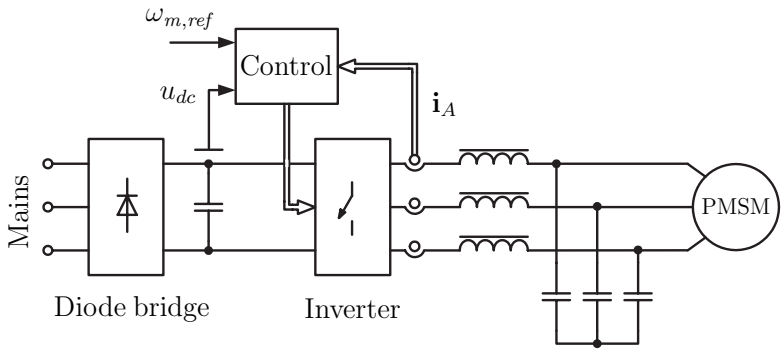

Figure 2.2: PMSM drive system equipped with inverter output LC filter.

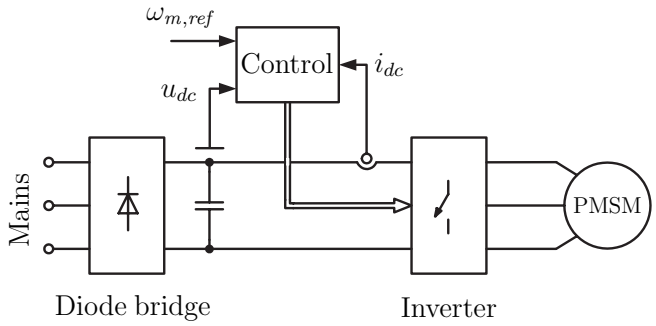

Figure 2.3: PMSM drive system with DC-link current measurement.

A block diagram of a PMSM drive equipped with inverter DC-link current measurement is shown in Fig. 2.3. The measured quantities are the inverter DC-link voltage u_{dc} and the DC-link current i_{dc}. The system with the DC-link current measurement is used in Publication **VIII**.

2.2 PMSM Model With Spatial Harmonics

The dynamic model of a PMSM is presented in the following. The well-known model (Krause et al., 2002) is complemented to include the spatial harmonics. Matrix notation is used because the rotor is salient and the inductances depend on the rotor position. The motor has no damping windings in the rotor. Using phase a, b, and c quantities, the electrical dynamics of the stator windings are expressed by voltage equation

$$\mathbf{u}_{abc} = R_s \mathbf{i}_{abc} + \dot{\boldsymbol{\psi}}_{abc} \tag{2.1}$$

where $\mathbf{u}_{abc} = [u_a \;\; u_b \;\; u_c]^T$ is the stator phase voltage vector, $\mathbf{i}_{abc} = [i_a \;\; i_b \;\; i_c]^T$ the phase current vector, and R_s the stator resistance. The stator flux linkage is

$$\boldsymbol{\psi}_{abc} = \mathbf{L}_{abc} \mathbf{i}_{abc} + \boldsymbol{\psi}_{pm,abc} \tag{2.2}$$

where

$$\boldsymbol{\psi}_{pm,abc} = \begin{bmatrix} \psi_{pm,a}(\theta_m) \\ \psi_{pm,b}(\theta_m) \\ \psi_{pm,c}(\theta_m) \end{bmatrix} \tag{2.3}$$

is the permanent magnet flux linkage vector. The phases flux linkages depend on the rotor electrical position θ_m, the variations being nearly sinusoidal functions of the position. The phase flux linkages differ from each other only in terms of phase shift: $\psi_{pm,b}(\theta_m) = \psi_{pm,a}(\theta_m - 2\pi/3)$ and $\psi_{pm,c}(\theta_m) = \psi_{pm,a}(\theta_m + 2\pi/3)$. The phase inductance matrix is

$$\mathbf{L}_{abc} = \begin{bmatrix} L_{aa}(\theta_m) & M_{ab}(\theta_m) & M_{ac}(\theta_m) \\ M_{ba}(\theta_m) & L_{bb}(\theta_m) & M_{bc}(\theta_m) \\ M_{ca}(\theta_m) & M_{cb}(\theta_m) & L_{cc}(\theta_m) \end{bmatrix} \tag{2.4}$$

where the phase self inductances are denoted by L and the mutual inductances between phases are denoted by M. The inductances have average components, and in salient machines, they also depend on the rotor position. The inductance matrix is symmetrical, and thus $M_{ba}(\theta_m) = M_{ab}(\theta_m)$, $M_{cb}(\theta_m) = M_{bc}(\theta_m)$, and $M_{ca}(\theta_m) = M_{ac}(\theta_m)$.

The self inductances are phase shifted as $L_{bb}(\theta_m) = L_{aa}(\theta_m - 2\pi/3)$ and $L_{cc}(\theta_m) = L_{aa}(\theta_m + 2\pi/3)$. Correspondingly, the phase shifts between the mutual inductances are $M_{ac}(\theta_m) = M_{bc}(\theta_m - 2\pi/3)$ and $M_{ab}(\theta_m) = M_{bc}(\theta_m + 2\pi/3)$.

More specifically, the phase flux linkages and the self and mutual inductances consist of certain harmonics of the rotor position θ_m. The flux linkage of phase a induced by the permanent magnets has a fundamental term and odd harmonics, i.e.

$$\psi_{pm,a} = \sum_{k=1,3,5\ldots} \psi_k \cos(k\theta_m) \tag{2.5}$$

If no zero-sequence component exists in the phase flux linkages, the factors ψ_k for values of k multiple of three are zero. Besides the fundamental $(k = 1)$, the most significant harmonics are the fifth and the seventh. The self and mutual inductances of the phases have an average component and even harmonics, i.e.

$$L_{aa} = \sum_{k=0,2,4\ldots} L_k \cos(k\theta_m) \tag{2.6}$$

$$M_{bc} = \sum_{k=0,2,4\ldots} M_k \cos(k\theta_m) \tag{2.7}$$

Fig. 2.4 shows one measured self inductance and one measured mutual inductance of the 2.2-kW machine described in Chapter 4. For the measurements, the delta connection of the stator winding was disconnected, and phases b and c were open-circuited. The measurements were made by supplying an alternating voltage having frequency of 50 Hz and voltage of 28 V (rms) to the winding of phase a. The current of phase a and the voltages of phases a and c were measured. The phase a self inductance and the mutual inductance between phases a and c were calculated by

$$L_a = \frac{1}{2\pi f}\sqrt{\frac{U_a^2}{I_a^2} - R_a^2}$$

$$M_{ac} = \frac{U_c}{2\pi f I_a}$$

respectively, where U_a is the rms voltage of phase a, I_a is the rms current of phase a, U_c is the rms voltage of phase c, R_a is the measured resistance of phase a, and f is the frequency. The inductances were measured at intervals of five electrical degrees. The modeled inductances consisting of the average component, the second harmonic, and the fourth harmonic calculated from the measured inductances using Fourier analysis are shown. The harmonics having a higher order are negligible in this machine.

Coordinate Transformation

The three phases of the stator winding are usually either delta-connected or the neutral point of the wye-connected winding is not connected. Hence, the zero-sequence components of the stator current and the stator voltage can be omitted, and the motor model can be expressed using two-axis quantities. A vector $\mathbf{u}_{abc} = [u_a \quad u_b \quad u_c]^T$ of stator phase quantities can be converted to a vector $\mathbf{u}_s^s = [u_\alpha \quad u_\beta]^T$ of orthogonal two-axis quantities in stationary reference frame.

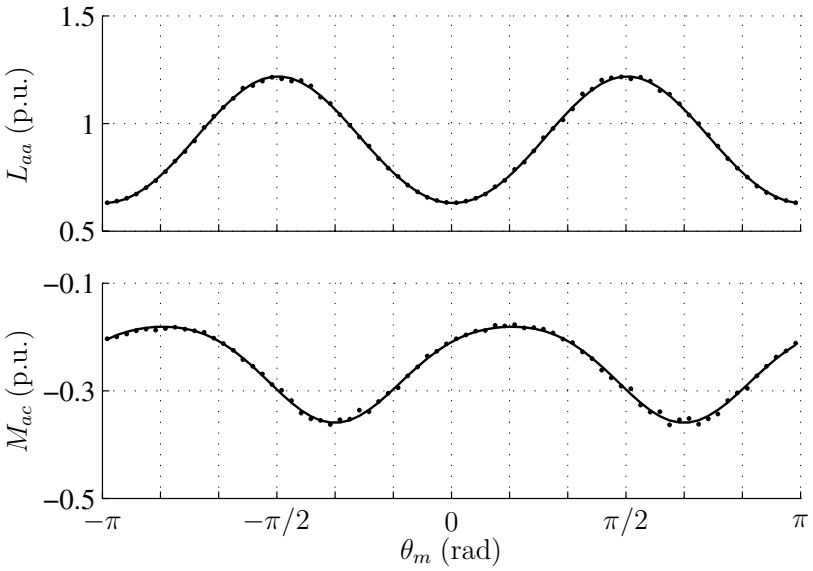

Figure 2.4: Measured (dots) and modeled (lines) inductances of the permanent magnet motor described in Chapter 4. First subplot shows self inductance L_{aa} and second subplot shows mutual inductance M_{ac}.

The quantities can be transformed into a reference frame having an arbitrary position. The quantities of a PMSM are usually expressed in the rotor reference frame that is aligned at electrical position θ_m. Here, the d axis of the rotor reference frame is aligned at the permanent magnet flux. For the vectors $\mathbf{u}_s = [u_d \quad u_q]^T$ and $\mathbf{u}_s^s = [u_\alpha \quad u_\beta]^T$, denoting the stator voltage in the rotor reference frame and in the stationary reference frame, respectively, the transformations are carried out by

$$\mathbf{u}_s = \mathbf{T}(-\theta_m)\mathbf{u}_s^s \tag{2.8a}$$
$$\mathbf{u}_s^s = \mathbf{T}(\theta_m)\mathbf{u}_s \tag{2.8b}$$

where

$$\mathbf{T}(\theta_m) = \cos(\theta_m)\mathbf{I} + \sin(\theta_m)\mathbf{J} \tag{2.9}$$

is the coordinate transformation matrix. For this matrix, $\mathbf{T}^{-1}(\theta_m) = \mathbf{T}(-\theta_m)$ applies, and the notation $e^{\mathbf{J}\theta_m} = \mathbf{T}(\theta_m)$ is often associated with the coordinate transformation. The matrices

$$\mathbf{I} = \begin{bmatrix} 1 & 0 \\ 0 & 1 \end{bmatrix}, \quad \mathbf{J} = \begin{bmatrix} 0 & -1 \\ 1 & 0 \end{bmatrix}$$

are the identity matrix and the orthogonal rotation matrix, respectively. It is to be noted that $\mathbf{J}^{-1} = -\mathbf{J}$ and $\mathbf{J}\mathbf{J} = -\mathbf{I}$, similarly to the imaginary unit j associated with complex variables. The three-phase stationary-reference-frame quantities can be transformed straight

into the two-axis rotor-reference-frame quantities, and vice versa, by using matrices:

$$\mathbf{u}_s = \underbrace{\frac{2}{3}\begin{bmatrix} \cos(-\theta_m) & \cos(-\theta_m + \frac{2\pi}{3}) & \cos(-\theta_m - \frac{2\pi}{3}) \\ \sin(-\theta_m) & \sin(-\theta_m + \frac{2\pi}{3}) & \sin(-\theta_m - \frac{2\pi}{3}) \end{bmatrix}}_{\mathbf{T}_{dq}} \mathbf{u}_{abc} \tag{2.10a}$$

$$\mathbf{u}_{abc} = \underbrace{\begin{bmatrix} \cos(\theta_m) & -\sin(\theta_m) \\ \cos(\theta_m - \frac{2\pi}{3}) & -\sin(\theta_m - \frac{2\pi}{3}) \\ \cos(\theta_m + \frac{2\pi}{3}) & -\sin(\theta_m + \frac{2\pi}{3}) \end{bmatrix}}_{\mathbf{T}_{abc}} \mathbf{u}_s \tag{2.10b}$$

respectively.

Using the matrices $\mathbf{T}_{dq}$ and $\mathbf{T}_{abc}$, the motor model expressed using phase quantities can be transformed into a two-axis model in the rotor reference frame. The voltage equation (2.1) is transformed by multiplying from the left-hand side by $\mathbf{T}_{dq}$, i.e.

$$\mathbf{T}_{dq}\mathbf{u}_{abc} = R_s\mathbf{T}_{dq}\mathbf{i}_{abc} + \mathbf{T}_{dq}\frac{d}{dt}\left(\boldsymbol{\psi}_{abc}\right) \tag{2.11}$$

For transforming the stator flux into the rotor reference frame, the flux vector inside the parentheses is multiplied with the matrix product $\mathbf{T}_{abc}\mathbf{T}_{dq}$ from the left hand side. When the two-axis rotor-reference-frame vectors for the stator voltage $\mathbf{u}_s$, the stator current $\mathbf{i}_s$, and the stator flux $\boldsymbol{\psi}_s$ are also introduced, the result is

$$\mathbf{u}_s = R_s\mathbf{i}_s + \mathbf{T}_{dq}\frac{d}{dt}\left(\mathbf{T}_{abc}\boldsymbol{\psi}_s\right) \tag{2.12}$$

Applying the product differentiation rule gives

$$\mathbf{u}_s = R_s\mathbf{i}_s + \mathbf{T}_{dq}\dot{\mathbf{T}}_{abc}\boldsymbol{\psi}_s + \mathbf{T}_{dq}\mathbf{T}_{abc}\dot{\boldsymbol{\psi}}_s \tag{2.13}$$

Since $\dot{\mathbf{T}}_{abc} = \omega_m\mathbf{T}_{abc}\mathbf{J}$ and $\mathbf{T}_{dq}\mathbf{T}_{abc} = \mathbf{I}$, the voltage equation in the rotor reference frame

$$\mathbf{u}_s = R_s\mathbf{i}_s + \dot{\boldsymbol{\psi}}_s + \omega_m\mathbf{J}\boldsymbol{\psi}_s \tag{2.14}$$

finally results, where ω_m is the electrical angular speed of the rotor.

For transforming the flux equation (2.2), a similar multiplication is applied, i.e.

$$\mathbf{T}_{dq}\boldsymbol{\psi}_{abc} = \mathbf{T}_{dq}\mathbf{L}_{abc}\mathbf{i}_{abc} + \mathbf{T}_{dq}\boldsymbol{\psi}_{pm,abc} \tag{2.15}$$

For transforming the stator current $\mathbf{i}_{abc}$ into the rotor reference frame, it is multiplied by the matrix product $\mathbf{T}_{abc}\mathbf{T}_{dq}$ from the left-hand side. Using quantities expressed in the rotor reference frame, the result is

$$\boldsymbol{\psi}_s = \mathbf{L}_s\mathbf{i}_s + \boldsymbol{\psi}_{pm} \tag{2.16}$$

where the permanent magnet flux vector and the stator inductance matrix are

$$\boldsymbol{\psi}_{pm} = \mathbf{T}_{dq}\boldsymbol{\psi}_{pm,abc} \tag{2.17}$$

$$\mathbf{L}_s = \mathbf{T}_{dq}\mathbf{L}_{abc}\mathbf{T}_{abc} \tag{2.18}$$

respectively.

If the spatial harmonics in the permanent magnet flux and in the stator inductance are omitted, the permanent magnet flux in (2.3) consists of only a fundamental component in

the stationary reference frame, forming a positive-sequence system. In the rotor reference frame, only a constant on the d axis results, i.e.

$$\boldsymbol{\psi}_{pm} = \begin{bmatrix} \psi_{pm0} \\ 0 \end{bmatrix} \tag{2.19}$$

where ψ_{pm0} is the flux linkage amplitude. The averages of the stator inductances in (2.4) appear as constants when transformed into the rotor reference frame. The second harmonic in the stationary reference frame results in a difference between the inductances on the d and q axes. In the rotor reference frame, this anisotropy in the inductance is independent on the rotor position, and is often referred to as saliency. The inductance is thus

$$\mathbf{L}_s = \begin{bmatrix} L_d & 0 \\ 0 & L_q \end{bmatrix} \tag{2.20}$$

where L_d and L_q are synchronous d- and q-axis inductances, respectively.

If the harmonics are taken into account, (2.19) and (2.20) become more complicated. For the permanent magnet flux, the fifth and the seventh harmonics in the stationary reference frame form negative- and positive-sequence systems, respectively, and are both transformed into sixth harmonics in the rotor reference frame. The resulting permanent magnet flux vector in the rotor reference frame is expressed as (Low et al., 1990)

$$\boldsymbol{\psi}_{pm} = \begin{bmatrix} \psi_{pm0} + \psi_{d6}\cos(6\theta_m) \\ \psi_{q6}\sin(6\theta_m) \end{bmatrix} \tag{2.21}$$

where harmonics of order higher than six are omitted. The amplitudes of the sixth harmonics on the d and q axes are denoted by ψ_{d6} and ψ_{q6}, respectively. For the stator inductance, the fourth harmonic in (2.4) is transformed into the sixth harmonic in the rotor reference frame. The resulting inductance matrix is (Low et al., 1990)

$$\mathbf{L}_s = \begin{bmatrix} L_d + L_6\cos(6\theta_m) & -L_6\sin(6\theta_m) \\ -L_6\sin(6\theta_m) & L_q - L_6\cos(6\theta_m) \end{bmatrix} \tag{2.22}$$

in the rotor reference frame, where L_6 is the amplitude of the inductance sixth harmonic.

Electromagnetic Torque

If the harmonics in the permanent magnet flux and in the stator inductance are omitted, the electromagnetic torque is

$$T_e = \frac{3p}{2}\boldsymbol{\psi}_s^T\mathbf{J}^T\mathbf{i}_s \tag{2.23}$$

where p is the number of pole pairs in the motor. The torque is thus proportional to the stator flux and to the stator current component that is perpendicular to the stator flux. Written in component form in terms of the stator current, the electromagnetic torque is

$$T_e = \frac{3p}{2}\left[\psi_{pm0}i_q + (L_d - L_q)i_d i_q\right] \tag{2.24}$$

When the spatial variations of the permanent magnet flux and the inductance are not sinusoidal, (2.23) no longer holds. The torque can be solved from the energy equilibrium instead. The magnetic field energy is (Krause et al., 2002)

$$W_f = \frac{1}{2}\mathbf{i}_{abc}^T\mathbf{L}_{abc}\mathbf{i}_{abc} + \mathbf{i}_{abc}^T\boldsymbol{\psi}_{pm,abc} \tag{2.25}$$

The torque is the magnetic co-energy W_c differentiated with respect to the mechanical rotor position. When linear magnetics are assumed, $W_c = W_f$, and the torque is

$$T_e = \frac{dW_f}{d(\theta_m/p)} \tag{2.26}$$

Assuming that the stator phase currents are not dependent on the rotor position, the torque becomes

$$T_e = p\left[\frac{1}{2}\mathbf{i}_{abc}^T \frac{d}{d\theta_m}(\mathbf{L}_{abc})\mathbf{i}_{abc} + \mathbf{i}_{abc}^T \frac{d}{d\theta_m}\boldsymbol{\psi}_{pm,abc}\right] \tag{2.27}$$

The transformation into the two-phase quantities in the rotor reference frame is carried out by the coordinate transformation matrices in (2.10a) and (2.10b), yielding

$$\begin{aligned} T_e = p\Bigg[&\frac{1}{2}(\mathbf{T}_{abc}\mathbf{i}_s)^T \frac{d}{d\theta_m}(\mathbf{T}_{abc}\mathbf{L}_s\mathbf{T}_{dq})(\mathbf{T}_{abc}\mathbf{i}_s) \\ &+ (\mathbf{T}_{abc}\mathbf{i}_s)^T \frac{d}{d\theta_m}(\mathbf{T}_{abc}\boldsymbol{\psi}_{pm})\Bigg] \end{aligned} \tag{2.28}$$

The product differentiation rule is applied to (2.28). Since $(\mathbf{T}_{abc}\mathbf{i}_s)^T = \mathbf{i}_s^T\mathbf{T}_{abc}^T$, $\frac{d}{d\theta_m}\mathbf{T}_{dq} = -\mathbf{J}\mathbf{T}_{dq}$, and $\frac{d}{d\theta_m}\mathbf{T}_{abc} = \mathbf{T}_{abc}\mathbf{J}$, the torque can be written as (Madani et al., 1995)

$$\begin{aligned} T_e = \frac{3p}{2}\mathbf{i}_s^T\Bigg[&\frac{1}{2}\left(\mathbf{J}\mathbf{L}_s + \frac{d}{d\theta_m}\mathbf{L}_s - \mathbf{L}_s\mathbf{J}\right)\mathbf{i}_s \\ &+ \mathbf{J}\boldsymbol{\psi}_{pm} + \frac{d}{d\theta_m}\boldsymbol{\psi}_{pm}\Bigg] \end{aligned} \tag{2.29}$$

The torque can be expressed in component form by substituting (2.21) and (2.22) for the permanent magnet flux and the stator inductance, respectively, in (2.29). The result is

$$\begin{aligned} T_e = \frac{3p}{2}\big\{&\psi_{pm0}i_q + (L_d - L_q)i_d i_q \\ &- 2L_6\sin(6\theta_m)(i_d^2 - i_q^2) - 4L_6\cos(6\theta_m)i_d i_q \\ &+ i_q\cos(6\theta_m)(\psi_{d6} + 6\psi_{q6}) - i_d\sin(6\theta_m)(\psi_{q6} + 6\psi_{d6})\big\} \end{aligned} \tag{2.30}$$

The estimation of the electromagnetic torque in Publications **IV** and **V** is based on this equation.

2.3 Magnetic Saturation

In the motor model described above, the inductances L_d and L_q of the PMSM have been assumed to be constant. In actual machines, however, the iron gets saturated as the magnetic flux increases. Thus, depending on the currents of the machine, the saturation effect changes the inductances. If the saturation is not taken into account in the machine model, the resulting mismatch in the inductances degrades performance and causes estimation errors.

Magnetic saturation is a well-recognized problem and has been under investigation for decades. Models for saturation have earlier been proposed for electrically excited synchronous machines (Xie and Ramshaw, 1986), principally applicable also to PMSMs. The

simplest way to model the saturation is to consider the d- and q-axis inductances independent of the current on the perpendicular axis. The stator flux linkages can be then modeled by

$$\psi_{sd} = L_d(i_d)i_d + \psi_{pm} \tag{2.31a}$$
$$\psi_{sq} = L_q(i_q)i_q \tag{2.31b}$$

This type of representation is not always sufficient, because it omits the magnetic cross coupling between the orthogonal axes. This cross-saturation phenomenon, verified experimentally in an induction motor by Vas et al. (1986), can be significant also in interior-magnet PMSMs (Stumberger et al., 2003). The saturation is sometimes modeled using only a single saturation factor (Boldea and Nasar, 1988; Melkebeek and Willems, 1990), usually determined by the resultant magnetizing current. In this case, the stator flux linkages are

$$\psi_{sd} = L_d(i_m)i_d + \psi_{pm} \tag{2.32a}$$
$$\psi_{sq} = L_q(i_m)i_q \tag{2.32b}$$

where

$$i_m = \sqrt{i_d^2 + K^2 i_q^2} \tag{2.33}$$

is the resultant magnetizing current, K being a constant. In these models, the d and q components of the current affect the stator flux components on the perpendicular axes, and the cross-saturation is thus taken into account. Different ways to model the stator inductances as functions of the currents are presented by Bianchi and Bolognani (1998). The stator inductances can also be modeled as functions of the magnetic flux (de Jong, 1980).

The interior-magnet PMSM used in the experiments of this thesis and described in detail in Chapter 4 is an experimental motor, being a larger-size machine than necessary. Experimental identification of the saturation of the d- and q-axis inductances has revealed that the inductances remain nearly unchanged even when 150 % of the nominal current is applied. Hence, experimental verification of saturation models would have been difficult.

2.4 Inverter Output Filter Model

In the presence of an inverter output LC filter, the chokes and the capacitors of the filter increase the complexity of the system dynamics. In addition to the PMSM, the dynamics of the filter have to be modeled. The dynamic equations of the LC filter inductor and capacitor in the rotor reference frame are

$$\mathbf{u}_A - \mathbf{u}_s = R_{Lf}\mathbf{i}_A + L_f\dot{\mathbf{i}}_A + \omega_m L_f \mathbf{J}\mathbf{i}_A \tag{2.34}$$
$$\mathbf{i}_A - \mathbf{i}_s = C_f\dot{\mathbf{u}}_s + \omega_m C_f \mathbf{J}\mathbf{u}_s \tag{2.35}$$

respectively, where $\mathbf{i}_A = [i_{Ad} \quad i_{Aq}]^T$ is the inverter output current, $\mathbf{u}_A = [u_{Ad} \quad u_{Aq}]^T$ the inverter output voltage, L_f the inductance and R_{Lf} the series resistance of the filter inductor, and C_f is the filter capacitance.

Chapter 3

Sensorless Vector Control

The methods for the speed and position estimation of PMSMs can be divided into two groups: fundamental-excitation methods based on the detection of the rotor back-emf and signal injection methods detecting the magnetic anisotropy of the PMSM. Combined methods, or hybrid methods, use both of these types and usually change the method as the rotor speed varies. This chapter reviews these methods and discusses the different techniques for sensorless control. Motor parameter estimators are briefly reviewed, and compensation of the electromagnetic torque ripple is discussed. Sensorless control of drives equipped with an inverter output filter and DC-link current measurement is also dealt with.

3.1 Fundamental-Excitation Methods

A common way for the speed estimation of an electric motor is the back-emf detection based on a model of the machine (Xu and Novotny, 1991). These methods are often referred to as model-based, or fundamental-excitation methods. Some of the methods designed for induction motors are applicable to PMSMs with minor changes. The estimation methods for PMSMs can also be applied to synchronous reluctance motors (Lagerquist et al., 1994), which can principally be considered as PMSMs without the permanent magnets in the rotor.

A wide variety of fundamental-excitation methods exist for PMSMs. One alternative is to use a voltage model for the estimation of the stator flux, and to calculate the rotor position estimate using the angle of the estimated flux (Wu and Slemon, 1991; Consoli et al., 1994). The voltage model is based on simulation of the stator voltage equation, basically by estimating the stator flux as an integral of the back-emf. Due to the presence of parameter errors and measurement noise, the open-loop integration results in integrator drift that has to be compensated for. Ertugrul and Acarnley (1994) used integration of the phase voltages and currents to estimate the flux linkages, and introduced correction terms to compensate for the integrator drift. An extended Kalman filter can be applied for the state estimation of a PMSM (Sattler and Stärker, 1989; Dhaouadi et al., 1991; Bolognani et al., 1999). Extended Kalman filters are recursive filters for nonlinear systems, and suited for use with noisy measurements. For the salient-rotor PMSMs, extended emf models have been proposed by Morimoto et al. (2002) and Chen et al. (2003). The idea of the extended emf is to include the saliency in the back-emf, in which case the saliency vanishes from the modeled stator inductance. The saliency can also be included in a fictitious permanent magnet flux (Koonlaboon and Sangwongwanich, 2005), leading to a model in which the

salient machine can also be treated in a fashion similar to a non-salient machine.

A state observer for a salient PMSM was proposed by Jones and Lang (1989). The observer included two states for the electrical dynamics and two states, the rotor speed and position, for the mechanical dynamics. Park and Lee (1989) used an observer for the electrical dynamics, but the rotor speed was estimated using an adaptation mechanism instead of a mechanical model in the state observer. An alternative to the speed adaptation is to determine the rotor position directly from the back-emf using the arctan function (Kim and Sul, 1995; Chen et al., 2003). The rotor speed can be determined by differentiating the rotor position estimate, but the resulting noisy speed estimate has to be filtered. Instead of the differentiation, Kim and Sul (1995) estimated the rotor speed using the back-emf and the rotor flux estimates, and Chen et al. (2003) using an adaptation mechanism. In these methods, the rotor position estimation is independent of the rotor speed estimation. Hence, the estimated rotor position is not necessarily the integral of the estimated rotor speed, and a steady-state speed estimation error may result.

In an adaptive observer, the electrical dynamics is modeled using at least two states, and the rotor speed is estimated using a speed adaptation mechanism. In connection with the estimation of the electrical states, a PI-type speed adaptation mechanism was proposed for induction motor drives by Kubota et al. (1993), and for PMSM drives by Yang et al. (1993). The adaptation mechanism can also be nonlinear: Furuhashi et al. (1992) used a sliding-mode observer with a signum function in the adaptation mechanism.

While the electrical dynamics can be modeled in different ways, the existence of the speed adaptation mechanism divides the observers into two groups. Using an adaptation mechanism instead of modeling the mechanics is reasonable since it is difficult to determine the mechanical parameters. In this thesis, modified voltage models (Publication **I**) and adaptive observers with rotor speed adaptation (Publications **II** and **III**) are investigated in more detail.

3.1.1 Modified Voltage Models

The voltage model is a simple means to estimate the rotor flux of an AC machine. The principle is to use the stator voltage equation to estimate either the stator flux or the rotor flux (or the permanent magnet flux in PMSMs). The rotor speed and position are further calculated from the flux estimate. The motor dynamics can be modeled either in the stationary reference frame or in the rotor reference frame.

In the stationary reference frame, the stator voltage expressed by the estimated quantities is

$$\mathbf{u}_s^s = \hat{R}_s \mathbf{i}_s^s + \frac{d}{dt}\hat{\boldsymbol{\psi}}_s^s \tag{3.1}$$

where estimates are marked by $\hat{}$ and superscript s denotes the stator reference frame. Wu and Slemon (1991) proposed a sensorless method for PMSMs, where the stator flux is estimated using (3.1), and the voltage model is modified to compensate the drift caused by open-loop integration. The rotor position and speed are calculated from the estimated stator flux. By substituting (2.16) expressed in terms of stator-reference-frame quantities for the stator flux in (3.1),

$$\frac{d}{dt}\hat{\boldsymbol{\psi}}_{pm}^s = \underbrace{\mathbf{u}_s^s - \hat{R}_s \mathbf{i}_s^s - \frac{d}{dt}(\hat{\mathbf{L}}_s^s \mathbf{i}_s^s)}_{\hat{\mathbf{E}}_f^s} \tag{3.2}$$

is obtained for the dynamics of the estimated permanent magnet flux, $\hat{\mathbf{E}}_f^s$ being the estimate of the rotor back-emf. (3.2) can be used for the permanent magnet flux estimation if the drift caused by the open-loop integration is compensated for.

For salient PMSMs, (3.2) is not practical because the derivative of the stationary-reference-frame stator inductance $\hat{\mathbf{L}}_s^s$ in (3.2) is not zero. Hence, the stator voltage equation in the rotor reference frame (2.14) is applied to the estimated quantities, giving

$$\mathbf{u}_s' = \hat{R}_s \mathbf{i}_s' + \frac{d}{dt}\hat{\boldsymbol{\psi}}_s + \hat{\omega}_m \mathbf{J}\hat{\boldsymbol{\psi}}_s \tag{3.3}$$

where measured quantities expressed in the estimated rotor reference frame are marked by $'$. By writing (3.3) in terms of the stator current and the permanent magnet flux and rearranging, the voltage model now becomes

$$\frac{d}{dt}\hat{\boldsymbol{\psi}}_{pm} + \hat{\omega}_m \mathbf{J}\hat{\boldsymbol{\psi}}_{pm} = \underbrace{\mathbf{u}_s' - \hat{R}_s \mathbf{i}_s' - \hat{\mathbf{L}}_s \frac{d}{dt}\mathbf{i}_s' - \hat{\omega}_m \mathbf{J}\hat{\mathbf{L}}_s \mathbf{i}_s'}_{\hat{\mathbf{E}}_f} \tag{3.4}$$

where the derivative of the estimated permanent magnet flux has been taken into account, and $\hat{\mathbf{E}}_f = [\hat{e}_d \;\; \hat{e}_q]^T$ is the estimate of the rotor back-emf in the rotor reference frame. By writing (3.4) in component form and omitting the spatial harmonics in $\hat{\boldsymbol{\psi}}_{pm}$ and $\hat{\mathbf{L}}_s$,

$$\frac{d}{dt}\hat{\psi}_{pm} = \hat{e}_d \tag{3.5a}$$

$$\hat{\omega}_m = \frac{\hat{e}_q}{\hat{\psi}_{pm}} \tag{3.5b}$$

is obtained for the estimation of the permanent magnet flux and the rotor speed.

The pure voltage model in (3.5) cannot be used in practice for flux estimation due to the drift of the open-loop integration. A common solution to compensate for the drift is to replace the integration by a low-pass filter (Wu and Slemon, 1991). However, the low-pass filter introduces lag in the estimated flux. The resulting error can be compensated for in different ways. These variants of the pure voltage model in (3.5) are referred to as modified voltage models.

Shin et al. (2000) proposed the estimation of the stator flux of induction machines in the stator reference frame using a phase-shift factor for the lag compensation in connection with the low-pass filtering. Applied for the estimation of the permanent magnet flux, this modified voltage model is written as

$$\hat{\boldsymbol{\psi}}_{pm}^s = \frac{1}{s + \lambda|\hat{\omega}_m|}\left(\mathbf{I} - \operatorname{sgn}(\hat{\omega}_m)\lambda\mathbf{J}\right)\hat{\mathbf{E}}_f^s \tag{3.6}$$

where λ is a feedback gain, s is a differential operator, and the term $\lambda|\hat{\omega}_m|$ is the bandwidth of the low-pass filter. The approach leads to a model where the error in the estimated flux is ideally zero in steady state. Transforming (3.6) to the rotor reference frame and solving the flux derivative gives

$$\dot{\hat{\boldsymbol{\psi}}}_{pm} = \left(\mathbf{I} - \operatorname{sgn}(\hat{\omega}_m)\lambda\mathbf{J}\right)\hat{\mathbf{E}}_f - \left(\lambda|\hat{\omega}_m|\mathbf{I} + \hat{\omega}_m\mathbf{J}\right)\hat{\boldsymbol{\psi}}_{pm} \tag{3.7}$$

The estimates for the permanent magnet flux and the rotor speed can be solved from the components of (3.7) in a fashion similar to (3.5).

For the rotor flux estimation of induction motors, Ohtani et al. (1992) proposed the use of a compensation term that includes a reference value for the rotor flux. The method is also applicable to PMSMs when a presumed value of the permanent magnet flux is used in the compensation term. In this case, the modified voltage model is written as

$$\hat{\boldsymbol{\psi}}_{pm}^{s} = \frac{1}{s+\lambda}\hat{\mathbf{E}}_{f}^{s} + \frac{\lambda}{s+\lambda}\boldsymbol{\psi}_{pm,r}^{s} \tag{3.8}$$

in the stator reference frame, where $\boldsymbol{\psi}_{pm,r}^{s}$ is a presumed value of the permanent magnet flux and λ is the bandwidth of the low-pass filter used for the flux estimation. Transforming (3.8) into the estimated rotor reference frame yields

$$\dot{\hat{\boldsymbol{\psi}}}_{pm} = \hat{\mathbf{E}}_{f} - \hat{\omega}_{m}\mathbf{J}\hat{\boldsymbol{\psi}}_{pm} + \lambda\left(\boldsymbol{\psi}_{pm,r} - \hat{\boldsymbol{\psi}}_{pm}\right) \tag{3.9}$$

from which the permanent magnet flux and the rotor speed can be estimated in component form. The method in (3.9) was employed in the combined observer proposed in Publication **I**.

For comparison with the observers presented in the following subsection, (3.9) is written in terms of the estimated stator flux. By inserting the back-emf term from (3.4) into (3.9), the modified voltage model becomes

$$\dot{\hat{\boldsymbol{\psi}}}_{s} = \mathbf{u}_{s}' - \hat{R}_{s}\mathbf{i}_{s}' - \hat{\omega}_{m}\hat{\boldsymbol{\psi}}_{s} + \lambda\left(\boldsymbol{\psi}_{pm,r} - \hat{\boldsymbol{\psi}}_{pm}\right) \tag{3.10}$$

where the estimate for the permanent magnet flux is calculated using

$$\hat{\boldsymbol{\psi}}_{pm} = \hat{\boldsymbol{\psi}}_{s} - \hat{\mathbf{L}}_{s}\mathbf{i}_{s}' \tag{3.11}$$

In (3.10), the stator voltage and the stator current appear as inputs, and the negative feedback through $\hat{\boldsymbol{\psi}}_{pm}$ prevents the integrator drift. Compared to (3.9), (3.10) is more practical for the estimation of $\hat{\boldsymbol{\psi}}_{pm}$ because the derivative of the stator current, included in $\hat{\mathbf{E}}_{f}$, is not needed. Although the integrator drift is prevented in (3.9) and (3.10), the sensitivity to the motor parameter errors at low rotor speed remains.

3.1.2 Adaptive Observers

Adaptive observers, often referred to as model reference adaptive systems, are based on a dynamic model that mimics the AC motor. An adjustable model is used for estimating the system states—including the measured quantities—while the motor is considered as a reference model. The estimation error of a measured quantity is used in an adaptation mechanism that changes a quantity in the adjustable model such that the estimation error is driven to zero. In electric motors, the measured quantity is the stator current, and the estimate of the rotor speed or the rotor position is usually the quantity changed by the adaptation mechanism.

In the adaptive full-order observer proposed by Kubota et al. (1993) for sensorless induction motor drives, the stator current error is used for the rotor speed adaptation. A full-order observer for induction motors includes four electrical states since the rotor winding dynamics is also included. On the contrary, two states for the electrical dynamics should be sufficient for PMSMs. However, variants exist that include two additional states for the permanent magnet flux (Yang et al., 1993) or the back-emf (Kim and Sul, 1995) in the stator reference frame. These two additional states can be used for estimating the rotor position and the permanent magnet flux amplitude.

State Observer With Feedback Gain

The adaptive observer proposed by Yang et al. (1993) has four states that mimic the electrical dynamics and the rotor position, and it is implemented in the stator reference frame,

$$\frac{d}{dt}\begin{bmatrix} \hat{\mathbf{i}}_s^s \\ \hat{\boldsymbol{\psi}}_{pm}^s \end{bmatrix} = \begin{bmatrix} -(\hat{R}_s/\hat{L}_s)\mathbf{I} & -(\hat{\omega}_m/\hat{L}_s)\mathbf{J} \\ \mathbf{0} & \hat{\omega}_m\mathbf{J} \end{bmatrix}\begin{bmatrix} \hat{\mathbf{i}}_s^s \\ \hat{\boldsymbol{\psi}}_{pm}^s \end{bmatrix} + \begin{bmatrix} (1/\hat{L}_s)\mathbf{I} \\ \mathbf{0} \end{bmatrix}\mathbf{u}_s^s - \underbrace{\begin{bmatrix} \mathbf{G}_1 & \mathbf{0} \\ \mathbf{G}_2 & \mathbf{0} \end{bmatrix}}_{\mathbf{G}}\begin{bmatrix} \tilde{\mathbf{i}}_s^s \\ \tilde{\boldsymbol{\psi}}_{pm}^s \end{bmatrix} \tag{3.12}$$

where $\mathbf{G}$ is the observer gain, $\tilde{\mathbf{i}}_s^s = \mathbf{i}_s^s - \hat{\mathbf{i}}_s^s$ is the current estimation error, and $\tilde{\boldsymbol{\psi}}_{pm}^s = \boldsymbol{\psi}_{pm}^s - \hat{\boldsymbol{\psi}}_{pm}^s$ is the permanent magnet flux estimation error. The flux estimation error $\tilde{\boldsymbol{\psi}}_{pm}^s$ is not used in the estimation due to the zero matrices in the feedback gain $\mathbf{G}$. A non-salient machine is considered, and the stator inductance estimate $\hat{L}_s$ is thus a scalar parameter. The rotor speed estimate is obtained using a PI-type adaptation mechanism,

$$\hat{\omega}_m = k_p F_\varepsilon + k_i \int F_\varepsilon dt \tag{3.13}$$

k_p and k_i being the adaptation gains, and

$$F_\varepsilon = \hat{\boldsymbol{\psi}}_{pm}^{s\ T}\mathbf{J}\tilde{\mathbf{i}}_s^s \tag{3.14}$$

an error term used for the speed adaptation. The rotor position estimate is determined from the estimated permanent magnet flux components.

In (3.12), a non-salient machine has been assumed. The observer is not directly applicable to salient machines, because in that case the stator inductance is not constant in the stationary reference frame. For salient machines, the observer should be expressed either with the estimated stator flux as a state, or in the estimated rotor reference frame. Actually, both of these alternatives are beneficial:

- The inductance derivative can be omitted when stator flux estimate is selected as a state
- Saliency can be expressed without the rotor position estimate if the observer is expressed in the rotor reference frame

Moreover, it follows that it is easier to take the spatial harmonics or the magnetic saturation into account. Hence, both modifications are made to the observer. Transformed to the estimated rotor reference frame, the observer in (3.12) is

$$\frac{d}{dt}\begin{bmatrix} \hat{\mathbf{i}}_s \\ \hat{\boldsymbol{\psi}}_{pm} \end{bmatrix} = \begin{bmatrix} -(\hat{R}_s/\hat{L}_s)\mathbf{I} - \hat{\omega}_m\mathbf{J} & -(\hat{\omega}_m/\hat{L}_s)\mathbf{J} \\ \mathbf{0} & \mathbf{0} \end{bmatrix}\begin{bmatrix} \hat{\mathbf{i}}_s \\ \hat{\boldsymbol{\psi}}_{pm} \end{bmatrix} + \begin{bmatrix} (1/\hat{L}_s)\mathbf{I} \\ \mathbf{0} \end{bmatrix}\mathbf{u}_s' - \underbrace{\begin{bmatrix} \mathbf{G}_1 & \mathbf{0} \\ \mathbf{G}_2 & \mathbf{0} \end{bmatrix}}_{\mathbf{G}}\begin{bmatrix} \tilde{\mathbf{i}}_s \\ \tilde{\boldsymbol{\psi}}_{pm} \end{bmatrix} \tag{3.15}$$

When the stator flux is taken as a state variable and the permanent magnet flux estimate is considered as a constant parameter, the observer reduces to

$$\dot{\hat{\boldsymbol{\psi}}}_s = \mathbf{u}_s' - \hat{R}_s\hat{\mathbf{i}}_s - \hat{\omega}_m\mathbf{J}\hat{\boldsymbol{\psi}}_s - \hat{L}_s\mathbf{G}_1\tilde{\mathbf{i}}_s \tag{3.16}$$

where the stator current estimate is obtained using

$$\hat{\mathbf{i}}_s = (1/\hat{L}_s)\left(\hat{\boldsymbol{\psi}}_s - \hat{\boldsymbol{\psi}}_{pm}\right) \tag{3.17}$$

Written for a salient PMSM, the observer is

$$\dot{\hat{\boldsymbol{\psi}}}_s = \mathbf{u}'_s - \hat{R}_s\hat{\mathbf{i}}_s - \hat{\omega}_m\mathbf{J}\hat{\boldsymbol{\psi}}_s + \boldsymbol{\lambda}\tilde{\mathbf{i}}_s \tag{3.18}$$

$$\hat{\mathbf{i}}_s = \hat{\mathbf{L}}_s^{-1}\left(\hat{\boldsymbol{\psi}}_s - \hat{\boldsymbol{\psi}}_{pm}\right) \tag{3.19}$$

where $\boldsymbol{\lambda}$ denotes the observer gain. The adaptive observer used in Publication **III** is based on this model, and an error term

$$F_\varepsilon = \mathbf{C}_1\tilde{\mathbf{i}}_s \tag{3.20}$$

is used for the speed adaptation in (3.13), where $\mathbf{C}_1 = [0 \;\; \hat{L}_q]$. Hence, the current error q component is used for the adaptation, and the error term F_ε is proportional to the current error component perpendicular to the estimated permanent magnet flux, as in (3.14). The influence of the observer gain $\boldsymbol{\lambda}$ on the dynamic properties is investigated in Publication **III**. The observer of Publication **II** corresponds to (3.18), but the stator flux error is used for feedback and in the speed adaptation instead of the stator current error.

Publication **IV** deals with reduction of the effects of the spatial harmonics on the estimation. The harmonics are taken into account in the adaptive observer by including them in the the permanent magnet flux and the stator inductance estimates used for the calculation of the estimated stator current in (3.19). For the permanent magnet flux and the stator inductance, (2.21) and (2.22) are applied for the estimated quantities, respectively.

Observer With Correction Term

Andreescu (1999) proposed an adaptive observer where the stator flux is calculated using two models, a reference model and an adjustable model, and the flux error is used for the adaptation of the rotor position. The reference and adjustable models are

$$\dot{\hat{\boldsymbol{\psi}}}^s_{s,u} = \mathbf{u}^s_s - \hat{R}_s\mathbf{i}^s_s - \mathbf{u}^s_{corr} \tag{3.21a}$$

$$\hat{\boldsymbol{\psi}}^s_{s,i} = \mathbf{T}(\hat{\theta}_m)\left(\hat{\mathbf{L}}_s\mathbf{i}'_s + \hat{\boldsymbol{\psi}}_{pm}\right) \tag{3.21b}$$

respectively, where $\mathbf{T}(\hat{\theta}_m)$ is the coordinate transformation matrix from the estimated rotor reference frame to the stator reference frame. The correction term $\mathbf{u}^s_{corr}$, used to prevent the integration drift in the voltage model, is obtained using a PI mechanism, i.e.

$$\mathbf{u}^s_{corr} = \mathbf{K}_p\left(\hat{\boldsymbol{\psi}}^s_{s,i} - \hat{\boldsymbol{\psi}}^s_{s,u}\right) + \mathbf{K}_i\mathbf{u}^s_{corr,i} \tag{3.22a}$$

$$\frac{d}{dt}\mathbf{u}^s_{corr,i} = \hat{\boldsymbol{\psi}}^s_{s,i} - \hat{\boldsymbol{\psi}}^s_{s,u} \tag{3.22b}$$

where $\mathbf{K}_p$ and $\mathbf{K}_i$ are adaptation gain matrices. The rotor speed estimate is calculated using the PI-type speed adaptation mechanism in (3.13) and

$$F_\varepsilon = \frac{1}{\hat{\psi}^2_{pm}}\hat{\boldsymbol{\psi}}^s_{s,u}{}^T\mathbf{J}\hat{\boldsymbol{\psi}}^s_{s,i} \tag{3.23}$$

as the error term. The rotor position estimate needed for $\mathbf{T}(\hat{\theta}_m)$ in (3.21b) is calculated by integration from the rotor speed estimate.

For comparison with (3.18), the observer above is written in terms of the estimated stator flux $\hat{\boldsymbol{\psi}}_{s,u}$, the estimated stator current $\hat{\mathbf{i}}_s = \hat{\mathbf{L}}_s^{-1}(\hat{\boldsymbol{\psi}}_{s,u} - \hat{\boldsymbol{\psi}}_{pm})$, and the current estimation error $\tilde{\mathbf{i}}_s = \mathbf{i}'_s - \hat{\mathbf{i}}_s$. The correction term $\mathbf{u}_{corr,i}$ is considered as an additional state, (3.21b) is substituted for the flux $\hat{\boldsymbol{\psi}}^s_{si}$ in (3.22), and (3.22a) is substituted for the voltage $\mathbf{u}^s_{corr}$ in (3.21a). In the estimated rotor reference frame, the observer is

$$\begin{aligned}\frac{d}{dt}\begin{bmatrix} \hat{\boldsymbol{\psi}}_{s,u} \\ \mathbf{u}_{corr,i} \end{bmatrix} &= \begin{bmatrix} -\hat{\omega}_m\mathbf{J} & -\mathbf{K}_i \\ \mathbf{0} & -\hat{\omega}_m\mathbf{J} \end{bmatrix}\begin{bmatrix} \hat{\boldsymbol{\psi}}_{s,u} \\ \mathbf{u}_{corr,i} \end{bmatrix} \\ &\quad + \begin{bmatrix} \mathbf{u}'_s - \hat{R}_s\hat{\mathbf{i}}_s \\ \mathbf{0} \end{bmatrix} + \begin{bmatrix} -\hat{R}_s\mathbf{I} - \mathbf{K}_p\hat{\mathbf{L}}_s \\ \hat{\mathbf{L}}_s \end{bmatrix}\tilde{\mathbf{i}}_s \end{aligned} \tag{3.24}$$

The error term used in the speed adaptation written in terms of the estimated stator flux and the current estimation error is

$$F_\varepsilon = \frac{1}{\hat{\psi}^2_{pm}}\hat{\boldsymbol{\psi}}_{s,u}{}^T\mathbf{J}\hat{\mathbf{L}}_s\tilde{\mathbf{i}}_s \tag{3.25}$$

Hence, if the measured stator current $\mathbf{i}'_s$ is used as an input in (3.21) instead of the estimated stator current, an additional gain term $-\hat{R}_s\mathbf{I}$ results in (3.24) when the observer is written in terms of the estimated stator current. The PI mechanism used for the drift compensation is a complex way to stabilize the integration. A proper selection of the feedback gain is a more straightforward way to design an observer that has good dynamic properties.

3.2 Signal Injection Methods

Fundamental-excitation methods are based on the rotor back-emf that has to be distinguished from the measurement noise and the voltage drops over the stator resistance and the inductances. The back-emf is proportional to the rotor speed, while the measurement errors and the voltage drops remain constant. Hence, fundamental-excitation methods suffer from errors in the measurements and the motor parameter estimates, and the estimation becomes difficult at low speeds. At zero speed, the PMSM is unobservable since the back-emf is zero.

Signal injection methods offer a solution to the estimation problems at low speeds. Based on detecting the magnetic anisotropy, the signal injection methods can basically operate regardless of the rotor speed. A voltage or a current signal, having a frequency other than the fundamental, is injected into the motor. Correspondingly, the current or the voltage response, containing information on the anisotropy, can be used for detecting the rotor position.

Schroedl (1988) proposed the rotor position estimation via detecting the phase inductance variation during inverter switching pulses. Based on this approach, Schroedl (1996) developed the "INFORM" method, where a sequence of discrete voltage pulses is injected into the machine, and the rotor position estimate is deduced from the difference in the stator inductance. Kulkarni and Ehsani (1992) proposed another method, also based on the phase inductance variation, where the inductances were measured during normal operation of the PWM.

Another approach for detecting the saliency of the PMSM is to use a continuous excitation voltage. Jansen and Lorenz (1995) proposed the injection of a rotating HF voltage vector into the stator-reference-frame voltage reference. The HF excitation voltage is superimposed on the fundamental voltage reference. The rotor position information is included in the stator current component rotating in the negative direction at the excitation frequency. Demodulating the current signal results in an error signal proportional to the position estimation error. This error signal is used in an observer that estimates the rotor speed and position.

Instead of the rotating injection voltage, an alternating sinusoidal excitation voltage can be superimposed on the stator voltage reference in the estimated rotor reference frame. An alternating HF signal injection was first proposed by Yong et al. (1994) for induction motors. The idea of the method is to inject a current signal into the d axis of the estimated rotor flux reference frame. The estimation of the rotor flux position is based on the estimated torque ripple that results from erroneous flux position. The injection of an alternating HF voltage was proposed by Corley and Lorenz (1998) for interior-magnet PMSMs. In this method, the voltage is injected into the q axis of the estimated rotor reference frame, and the stator current d component is used for the rotor position estimation. The injection on the q axis results in smaller HF current compared to the injection on the d axis because $L_q > L_d$ in interior-magnet PMSMs. The injection of an alternating HF voltage on the d axis was proposed by Ha and Sul (1999) for induction motor drives. If the magnetic saliency is small, the injection on the d axis may be preferable to the injection on q axis, because the resulting torque ripple is smaller. Linke et al. (2002) used the injection of an HF voltage on the d axis for surface-magnet PMSMs.

The methods using discrete voltage pulses for the HF excitation do not necessarily need additional voltage components if the inverter switching pulses are used (Kulkarni and Ehsani, 1992). However, they cannot be used with a space-vector pulsewidth modulation (SVPWM) and current sampling that is synchronized with the modulation. In the method proposed by Schroedl (1996), the excitation of the fundamental voltage has to be interrupted when the HF voltage sequence is applied. On the other hand, the methods based on continuous excitation can be used with SVPWM and they do not interrupt the normal operation. The methods also provide an error signal that is approximately proportional to the position estimation error. The error signal is used in an adaptation mechanism, and the estimation dynamics can be affected by changing the adaptation gains. Due to the above mentioned restrictions related to the signal injection methods based on discrete voltage pulses and the advantages of the continuous-excitation methods, only methods using the continuous voltage excitation are investigated in this thesis.

Rotating Voltage Excitation

An HF signal injection method using rotating voltage as an excitation signal was first proposed by Jansen and Lorenz (1995). A voltage signal

$$\mathbf{u}_c^s = \hat{u}_c \mathbf{T}(\omega_c t) \begin{bmatrix} 1 \\ 0 \end{bmatrix} \tag{3.26}$$

is superimposed on the voltage reference in the stator reference frame. $\hat{u}_c$ is the amplitude of the rotating voltage and $\mathbf{T}(\omega_c t) = \cos(\omega_c t)\mathbf{I} + \sin(\omega_c t)\mathbf{J}$ is a coordinate transformation matrix, ω_c being the angular frequency of the excitation signal.

To solve the resulting HF stator current, the relationship between the current and the voltage is investigated. Since high frequencies are considered, the stator resistance and the back-emf are omitted, and the stator current derivative is

$$\frac{d}{dt}\mathbf{i}_s^s = \left(\mathbf{T}(\theta_m)\mathbf{L}_s^{-1}\mathbf{T}(-\theta_m)\right)\mathbf{u}_s^s \tag{3.27}$$

Substituting $\mathbf{u}_c^s$ from (3.26) for $\mathbf{u}_s^s$ in (3.27) and integrating results in

$$\mathbf{i}_s^s = \frac{\hat{u}_c}{\omega_c}\left(\mathbf{T}(\theta_m)\mathbf{L}_s^{-1}\mathbf{T}(-\theta_m)\right)\mathbf{T}(\omega_c t)\mathbf{J}\begin{bmatrix}1\\0\end{bmatrix} \tag{3.28}$$

where θ_m is considered constant. By splitting the stator inductance matrix into components, this current can be written as

$$\mathbf{i}_s^s = -\frac{1}{2L_dL_q}\frac{\hat{u}_c}{\omega_c}\left\{(L_d+L_q)\mathbf{T}(\omega_c t) + (L_d-L_q)\mathbf{T}(2\theta_m)\mathbf{T}(-\omega_c t)\right\}\begin{bmatrix}0\\1\end{bmatrix} \tag{3.29}$$

where the position information is included in $\mathbf{T}(2\theta_m)$. Hence, the current vector rotating in the negative direction contains the position information.

For obtaining the rotor position estimation error, the current is transformed to a reference frame that rotates in the negative direction at frequency $\omega_c - 2\hat{\omega}_m$. The result is

$$\begin{aligned}\mathbf{T}(-2\hat{\theta}_m)\mathbf{T}(\omega_c t)\mathbf{i}_s^s = -\frac{1}{2L_dL_q}\frac{\hat{u}_c}{\omega_c}\big\{&(L_d+L_q)\mathbf{T}(-2\hat{\theta}_m)\mathbf{T}(2\omega_c t)\\ &+ (L_d-L_q)\mathbf{T}(2\tilde{\theta}_m)\big\}\begin{bmatrix}0\\1\end{bmatrix}\end{aligned} \tag{3.30}$$

where $\mathbf{T}(\tilde{\theta}_m) = \cos(\tilde{\theta}_m)\mathbf{I} + \sin(\tilde{\theta}_m)\mathbf{J}$ is the coordinate transformation matrix from the rotor reference frame to the estimated rotor reference frame. The error signal is obtained as the low-pass filtered d component of the current (3.30):

$$\varepsilon = \underbrace{-\frac{L_q - L_d}{2L_dL_q}\frac{\hat{u}_c}{\omega_c}}_{K_\varepsilon}\sin(2\tilde{\theta}_m) \tag{3.31}$$

K_ε being the signal injection gain. This error signal is used in an observer that estimates the rotor speed and position.

Instead of extracting an error signal from the current (3.29), the rotor position estimate can be evaluated directly from the current response. Consoli et al. (2001) proposed a method based on detecting the maximum and minimum points of the high-frequency current signal $\mathbf{i}_s^{sT}\mathbf{i}_s^s$. The rotor position is deduced using look-up tables when peak values of $\mathbf{i}_s^{sT}\mathbf{i}_s^s$ are detected. Silva et al. (2003) proposed a method where an arctan function is used for the rotor position calculation from the current response (3.30).

Alternating Voltage Excitation

Because the magnetic anisotropy is relatively small in the interior-magnet machine used in this thesis, the injection of an alternating HF voltage on the d axis was selected. An alternating voltage

$$\mathbf{u}_c = \hat{u}_c\cos(\omega_c t)\begin{bmatrix}1\\0\end{bmatrix} \tag{3.32}$$

is superimposed on the stator voltage reference in the estimated rotor reference frame. Since high frequencies are considered, the back-emf and the resistive voltage drop are omitted, giving

$$\frac{d}{dt}\mathbf{i}'_s = \left[\mathbf{T}(\tilde{\theta}_m)\mathbf{L}_s^{-1}\mathbf{T}(-\tilde{\theta}_m)\right]\mathbf{u}'_s \tag{3.33}$$

for the relationship between the voltage and the current of the PMSM. The HF current response can be solved by substituting $\mathbf{u}_c$ for the voltage $\mathbf{u}'_s$ in (3.33) and by considering the rotor position error constant, yielding

$$\mathbf{i}'_s = \frac{\hat{u}_c}{\omega_c}\sin(\omega_c t)\left[\mathbf{T}(\tilde{\theta}_m)\mathbf{L}_s^{-1}\mathbf{T}(-\tilde{\theta}_m)\right]\begin{bmatrix}1\\0\end{bmatrix} \tag{3.34}$$

By splitting the stator inductance into components,

$$\mathbf{i}'_s = \frac{1}{2L_dL_q}\frac{\hat{u}_c}{\omega_c}\sin(\omega_c t)\left\{(L_d+L_q)\begin{bmatrix}1\\0\end{bmatrix} - (L_d-L_q)\begin{bmatrix}\cos(2\tilde{\theta}_m)\\ \sin(2\tilde{\theta}_m)\end{bmatrix}\right\} \tag{3.35}$$

is obtained for the HF stator current, where the position-dependent part can be distinguished.

The position error can be extracted from the current signal (3.35) in several ways. One possibility is to use the current component perpendicular to the voltage excitation (Corley and Lorenz, 1998). In (3.35), the q component of the current signal contains only a position-dependent term, which can be extracted by demodulating and low-pass filtering, i.e.

$$\varepsilon = \mathrm{LPF}\{\sin(\omega_c t)[\,0\;\;1\,]\mathbf{i}'_s\} \tag{3.36}$$

giving the error signal

$$\varepsilon = \underbrace{\frac{L_q - L_d}{4L_dL_q}\frac{\hat{u}_c}{\omega_c}}_{K_\varepsilon}\sin(2\tilde{\theta}_m) \tag{3.37}$$

where K_ε is the signal injection gain for this type of demodulation. This gain is only half of what is gained using the rotating injection in (3.31). However, it is to be noted that the voltage is injected both on the d and q axes in the rotating injection, contrary to the alternating injection.

Ha et al. (2003) proposed another type of demodulation with the alternating signal injection for PMSMs. The idea is to compare the high-frequency impedances at two orthogonal axes that are displaced by 45 degrees to the negative and positive directions, respectively, from the d axis of the estimated rotor reference frame. The stator current $\mathbf{i}'_s$ is first transformed to a reference frame lagging the estimated rotor reference frame by 45 electrical degrees, i.e.

$$\mathbf{i}_{sm} = \mathbf{T}(\pi/4)\mathbf{i}'_s \tag{3.38}$$

where $\mathbf{T}(\pi/4) = \mathbf{I}\cos(\pi/4) + \mathbf{J}\sin(\pi/4)$. The error signal is then calculated as the difference between the squares of the components of the current $\mathbf{i}_{sm}$ using

$$\varepsilon = \mathrm{LPF}\left\{|i_{smq}|^2 - |i_{smd}|^2\right\} \tag{3.39}$$

The resulting error signal is

$$\varepsilon = \frac{L_q - L_d}{8L_d^2L_q^2}\frac{\hat{u}_c^2}{\omega_c^2}\left\{2(L_d+L_q)\sin(2\tilde{\theta}_m) - (L_d-L_q)\sin(4\tilde{\theta}_m)\right\} \tag{3.40}$$

The gain between $\tilde{\theta}_m$ and ε is not directly comparable to that of (3.31) and (3.37). When the parameters of the interior PMSM described in Chapter 4 are used, (3.40) gives an error signal having a magnitude less than a half of (3.37).

In the rotating signal injection method, the HF voltage is injected on the q axis in addition to the d axis. The resulting q-axis current creates more torque ripple than the d-axis current, since the q-axis current contributes more to the torque production. The higher current RMS value of the rotating injection results in additional power losses. Moreover, the rotating injection is not symmetrical in terms of the rotating direction of the rotor, since the injection frequency in the rotor reference frame changes with the rotor speed. The alternating signal injection method with the demodulation scheme in (3.36) was selected for use in this thesis.

Effect of Saturation and Inverter Nonlinearities

The magnetic saturation in the permanent magnet motors described in Chapter 2 disturbs the signal injection methods and causes estimation errors. Since the methods are based on tracking the inductance variation, the effect of the saturation can be severe. If the spatial position of the saliency is displaced due to the saturation, position estimation errors result. The saliency can also disappear due to the saturation, making the signal injection methods incapable of estimating the rotor position. Differences in the rotor geometry can also have significant effects on the saturation and, consequently, on the rotor position estimation using signal injection methods (Bianchi et al., 2007).

It is possible to compensate for the effects of the magnetic saturation in sensorless control. Teske et al. (2000) suppressed the saliency caused by the magnetic saturation in sensorless induction motor drives by decoupling the saturation-induced current component. Teske et al. also proposed a self-commissioning scheme for identifying the saturation effects. Li et al. (2007) used a modified demodulation scheme in connection with an HF signal injection method in compensating for the effects of the magnetic cross-saturation in salient-rotor PMSM drives. In addition to the drawbacks, the saturation can also be exploited in the speed and position estimation of non-salient machines through high-frequency signal injection. The use of the saturation-induced saliencies has been proposed for sensorless induction motor drives by Jansen and Lorenz (1996), and for surface-magnet PMSM drives by Linke et al. (2002) and Jang et al. (2003).

Another source of disturbance in the signal injection methods is the nonlinearities in the inverter (Guerrero et al., 2005). The effects during the inverter dead time, that has to be applied to prevent inverter shoot-through, cause errors in the inverter output phase voltages (Jeong and Park, 1991). At high phase current values, the error in the phase voltages can be approximated as being proportional to a signum function of the phase current. At lower phase current values, the parasitic capacitances in the power devices of the inverter reduce the dead-time effect (Urasaki et al., 2005). When the phase current is close to zero, the back-emf contributes to the phase voltage due to a zero current clamping effect (Choi and Sul, 1995). In addition to the dead time effects, the voltage drops over the IGBTs and diodes contribute to the inverter output voltage errors (Schmirgel and Krah, 2005). The signal injection methods are more affected by the inverter nonlinearities than the resistive voltage drops. In this thesis, the inverter dead time effects and the power device voltage drops are compensated for using a simple feedforward compensation (Pedersen et al., 1993).

Reduction of the Effects of Spatial Harmonics

In the signal injection methods reviewed above, the stator inductance of the PMSM is assumed to have only a single sinusoidally distributed saliency that appears as a difference between the d- and q-axis inductances in the rotor reference frame. In practical machines, the spatial distribution of the stator inductance also has higher-order harmonics. The inductance harmonics are discussed in Chapter 2. In addition to the rotor-position-dependent inductance harmonics, additional saliencies are caused by magnetic saturation, and in induction motors, by the rotor slots. Multiple saliencies is a commonly used term when referring to the non-sinusoidal spatial variation of the stator inductance.

The high-frequency signal injection methods are sensitive to all anisotropies in the electrical machines. If good rotor position estimation accuracy is demanded, the effects caused by the multiple saliencies have to be compensated. Degner and Lorenz (1998) used a rotating voltage excitation, and decoupled the higher-order harmonics from the measured stator current prior to the demodulation in sensorless induction motor drives. As a result, the position estimation accuracy was improved compared to the conventional method.

The methods developed for induction motor drives could also be applied to PMSMs: the stator current response is processed in order to suppress the effects of the multiple saliencies. On the contrary, Publication **IV** of this thesis introduces an approach where the current demodulation remains unchanged, but the HF excitation voltage is modified for reducing the effects of the inductance harmonics.

In Publication **IV**, the effects of the inductance harmonics are compensated for as follows. For the relationship between the stator voltage and the stator current, (2.16) is substituted for the stator flux in (2.14), resulting in

$$\mathbf{u}_s = R_s\mathbf{i}_s + \mathbf{L}_s\dot{\mathbf{i}}_s + \dot{\mathbf{L}}_s\mathbf{i}_s + \dot{\boldsymbol{\psi}}_{pm} + \omega_m\mathbf{J}\mathbf{L}_s\mathbf{i}_s + \omega_m\mathbf{J}\boldsymbol{\psi}_{pm} \tag{3.41}$$

Since high frequencies are considered, the back-emf and the resistive voltage drop are omitted, and (3.41) reduces to

$$\mathbf{u}_s = \mathbf{L}_s\dot{\mathbf{i}}_s + \dot{\mathbf{L}}_s\mathbf{i}_s \tag{3.42}$$

The rotor-reference-frame stator current corresponding to the zero position estimation error can be solved from (3.35):

$$\mathbf{i}_s = \frac{\hat{u}_c}{\omega_c L_d}\sin(\omega_c t)\begin{bmatrix} 1 \\ 0 \end{bmatrix} \tag{3.43}$$

Inserting this current and the stator inductance in (2.22) into (3.42) gives the modified HF excitation voltage to be fed to the motor. Written for the estimated quantities, the voltage is

$$\begin{aligned}\mathbf{u}_c = {} & \hat{u}_c\cos(\omega_c t)\begin{bmatrix} 1 + (\hat{L}_6/\hat{L}_d)\cos(6\hat{\theta}_m) \\ -(\hat{L}_6/\hat{L}_d)\sin(6\hat{\theta}_m) \end{bmatrix} \\ & + \frac{\hat{\omega}_m}{\omega_c}\hat{u}_c\sin(\omega_c t)\begin{bmatrix} -5(\hat{L}_6/\hat{L}_d)\sin(6\hat{\theta}_m) \\ 1 - 5(\hat{L}_6/\hat{L}_d)\cos(6\hat{\theta}_m) \end{bmatrix}\end{aligned} \tag{3.44}$$

Hence, the effects of the inductance harmonics are compensated for by a simple modification in the HF excitation voltage. It is to be noted that in Publication **IV**, lower speeds are considered than those in the previous publications. Therefore, the effects of the harmonics are more pronounced since the ripple in the speed is less filtered in the system.

Rotor Position Tracking

The signal injection methods that produce an error signal require an adaptation mechanism for the speed and position estimation. For this purpose, tracking observers (Jansen and Lorenz, 1995) and Kalman filters (Parasiliti et al., 2002) have been used. The tracking observer of Fig. 3.1 proposed by Jansen and Lorenz (1995) is based on the mechanical subsystem model and uses estimated electromagnetic torque $\hat{T}_e$ feedforward for better dynamics. If the estimates of the mechanical parameters, i.e. the moment of inertia $\hat{J}$ and the mechanical damping $\hat{b}$, are close to their actual values, the observer principally provides zero-lag speed and position estimates when the electromagnetic torque changes rapidly. The drawback is that the parameter estimates are needed in general, and incorrect estimates degrade the dynamic performance. Furthermore, the estimated torque feedforward does not reject load torque transients. In addition, the three parameters K_1, K_2, and K_3 have to be tuned properly.

A simpler method for the estimation was proposed by Harnefors and Nee (2000). The observer is shown in Fig. 3.2, and it comprises only the proportional and integral gains γ_p and γ_i, respectively. This observer is used in Publication **I** with the alternating signal injection method. Tuning the gains γ_p and γ_i without the mechanical parameters is also investigated in Publication **I**.

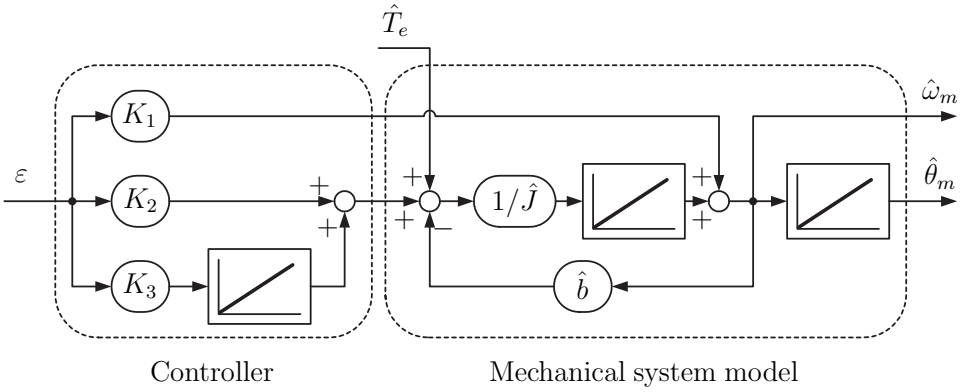

Figure 3.1: Rotor speed and position observer including mechanical system model.

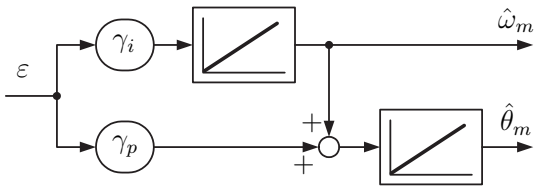

Figure 3.2: Rotor speed and position observer including proportional and integral parts.

3.3 Hybrid Methods

Combination of Voltage Model and Signal Injection

By combining a fundamental-excitation method and a signal injection method, the shortcomings of the methods can be avoided and the advantages can be exploited. These hybrid methods, or combined methods, use a fundamental-excitation method at medium and

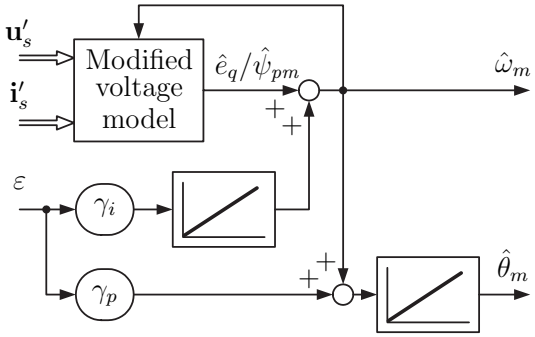

Figure 3.3: Modified voltage model combined with signal injection.

high speeds, and a signal injection method at low speeds, sometimes in connection with a fundamental-excitation method. Jansen and Lorenz (1996) discussed a method for sensorless induction motor drives, where a voltage model is used at high speeds and a signal injection method at low speeds. Silva et al. (2003) use weight coefficients to select the negative feedback for a voltage model in the transition region. At low speeds, a presumed value for the permanent magnet flux in the stationary reference frame is calculated using a rotor position estimate obtained from the signal injection method. This flux is used as a presumed value in the voltage model in a manner similar to (3.8).

A combination of a voltage model similar to that of used by Silva et al. (2003) and an HF signal injection method is proposed in Publication **I** of this thesis. The block diagram of the combined observer is shown in Fig. 3.3. The method incorporates the PI mechanism shown in Fig. 3.2. The influence of the HF signal injection is decreased with increasing speed, reaching zero in a certain speed limit. The modified voltage model operates in the whole speed range. The method is described in more detail in Publication **I**.

Combination of Adaptive Observer and Signal Injection

Adaptive observers and most signal injection methods with continuous excitation provide error signals, which are usually driven to zero in steady state using an adaptation mechanism. Tursini et al. (2003b) use an adaptive observer for the estimation at medium and high speeds, while the speed and position estimates are provided by a signal injection method at low speeds. The estimation method is simply changed at a certain speed. In order to obtain a smooth transition between the low-speed and medium-speed regions, the fundamental-excitation method and the signal injection method should be used simultaneously in at least a narrow speed range. It is not straightforward to combine the methods in the transition region, as two error signals giving different information have to be dealt with. Summing the outputs of two adaptation mechanisms for the rotor speed estimation is not sensible since the integrators of the adaptation mechanisms would diverge.

Ide et al. (2002) proposed a hybrid method for induction motor drives which employs a separate PI mechanism for both the fundamental-excitation method and the signal injection method . The error signals are fed through a high-pass filter and a low-pass filter, respectively. Since a high-pass filter is applied to the error signal from the fundamental-excitation method, the integral of the PI mechanism does not diverge. However, steady-state offset remains in that high-pass-filtered error signal. With adaptive observers, this would mean that a steady-state current estimation error is accepted.

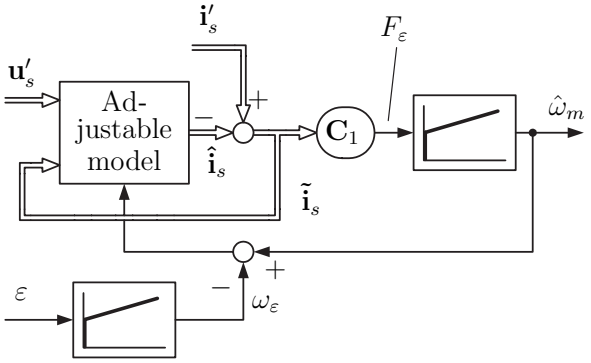

Figure 3.4: Adaptive observer combined with signal injection. Double lines indicate vector quantities whereas single lines indicate scalar quantities.

Aihara et al. (1999) suggested the addition of the error signals from the fundamental-excitation method and the signal injection method in a hybrid method for sensorless PMSM drives. Weight coefficients are used in the summation in a way that only the signal injection method is used at low speeds and only the fundamental-excitation method at medium and high speeds. Summation of the error signals in the transition region means that neither of the error signals is driven to zero in steady state. Even if the signal injection method has good accuracy, a steady-state position estimation error would result. Furthermore, the good dynamic properties of the fundamental-excitation method are not exploited at low speeds and standstill, because only the signal injection method is used for the estimation. Eskola (2006) proposed a hybrid method where weight coefficients are applied to the two error signals, but an additional speed term from a fundamental-excitation method is used in the whole speed range. As a result, the performance is improved at low speeds. Regarding the weighted summation of the error signals in the transition region, Wallmark and Harnefors (2006) investigated the stability of the estimation in order to determine design rules for the system.

In this thesis, a hybrid method is proposed, where an adaptive observer is used for the estimation throughout the whole speed range, and the estimation is augmented with an alternating HF signal injection method at low speeds. The block diagram of the combined observer is shown in Fig. 3.4. The signal injection method affects the adjustable model through a speed correction term ω_ε obtained using a PI mechanism

$$\omega_\varepsilon = \gamma_p \varepsilon + \gamma_i \int \varepsilon dt \tag{3.45}$$

from the error signal ε. The influence of the HF signal injection method is decreased as the speed increases. This hybrid method has the advantage that both error signals, F_ε and ε, are driven to zero in steady state. As the speed increases, the methods give inconsistent information and the PI-mechanism used with the signal injection method can drift in steady state. This drift can be avoided by limiting the speed correction term ω_ε to reasonable bounds. Details of the method are given in Publication **II**.

The two hybrid methods proposed within this thesis are not based on a change-over between the fundamental-excitation method and the signal injection method. Instead, the signal injection method is considered as a supplement to the fundamental-excitation method. It is to be noted that the fundamental-excitation method provides information regardless of the operating condition in both of the methods, and the combination is achieved through the use of a PI mechanism by which the error signal ε is driven to zero in steady state. Therefore, the methods have the following advantages:

- The good dynamic properties of the fundamental-excitation method are also available at low speeds and standstill
- The effect of the HF signal injection method can be altered by tuning the gains of the PI mechanism in (3.45)

The results shown in Fig. 9 in both Publications **I** and **II** can be used as an example for comparing the performance of the two hybrid methods. As the speed reference changes, the transient position error of the adaptive observer is smaller than that of the voltage model. Furthermore, the oscillations–mainly originating from the spatial harmonics in the motor–are damped by the adaptive observer more effectively. It is shown in Publication **III** that the properties of the adaptive observer can easily be affected by the observer gain. As a result, the performance is further improved. The combined observer of Fig. 3.4 is used in Publications **II**-**V** and with small modifications in Publications **VIII** and **IX**.

Convergence of Hybrid Speed and Position Estimation

It is difficult to prove the global convergence of speed and position estimation. However, the convergence can be investigated locally by linearizing the hybrid method of Fig. 3.4 and applying small-signal analysis.

The motor model without the spatial harmonics, expressed in the estimated rotor reference frame, is

$$\dot{\boldsymbol{\psi}}'_s = \mathbf{u}'_s - R_s\mathbf{i}'_s - \hat{\omega}_m\mathbf{J}\boldsymbol{\psi}'_s \tag{3.46a}$$
$$\mathbf{i}'_s = \mathbf{T}\mathbf{L}_s^{-1}\mathbf{T}^{-1}(\boldsymbol{\psi}'_s - \boldsymbol{\psi}'_{pm}) \tag{3.46b}$$

The hybrid observer is

$$\dot{\hat{\boldsymbol{\psi}}}_s = \mathbf{u}'_s - \hat{R}_s\hat{\mathbf{i}}_s - (\hat{\omega}_m - \omega_\varepsilon)\mathbf{J}\hat{\boldsymbol{\psi}}_s + \boldsymbol{\lambda}\tilde{\mathbf{i}}_s \tag{3.47a}$$
$$\hat{\mathbf{i}}_s = \hat{\mathbf{L}}_s^{-1}(\hat{\boldsymbol{\psi}}_s - \hat{\boldsymbol{\psi}}_{pm}) \tag{3.47b}$$

The adaptation mechanisms included in the observer are

$$\hat{\omega}_m = -\mathbf{k}_p\tilde{\mathbf{i}}_s - \mathbf{k}_i\int\tilde{\mathbf{i}}_s dt \tag{3.48a}$$
$$\omega_\varepsilon = \gamma_p\varepsilon + \gamma_i\int\varepsilon dt \tag{3.48b}$$

where $\mathbf{k}_p = [0 \quad k_p]$ and $\mathbf{k}_i = [0 \quad k_i]$ are the speed adaptation gain vectors and the error signal is approximated by a low-pass filter

$$\dot{\varepsilon} = \alpha_{lp}\big(2K_\varepsilon\tilde{\theta}_m - \varepsilon\big) \tag{3.49}$$

having bandwidth α_{lp}.

The dynamics of the stator flux error and the stator current estimation error are

$$\dot{\tilde{\boldsymbol{\psi}}}_s = -R_s\tilde{\mathbf{i}}_s - \hat{\omega}_m\mathbf{J}\tilde{\boldsymbol{\psi}}_s - \omega_\varepsilon\mathbf{J}\hat{\boldsymbol{\psi}}_s - \boldsymbol{\lambda}\tilde{\mathbf{i}}_s \tag{3.50a}$$
$$\tilde{\mathbf{i}}_s = \mathbf{T}\mathbf{L}_s^{-1}\mathbf{T}^{-1}(\boldsymbol{\psi}'_s - \mathbf{T}\boldsymbol{\psi}_{pm}) + \mathbf{L}_s^{-1}(\hat{\boldsymbol{\psi}}_s - \boldsymbol{\psi}_{pm}) \tag{3.50b}$$

where the motor parameter errors have been omitted. The system in (3.50) can be linearized around a certain operating point. The linearized system is

$$\dot{\tilde{\boldsymbol{\psi}}}_s = -\omega_{m0}\mathbf{J}\tilde{\boldsymbol{\psi}}_s - (R_s\mathbf{I} + \boldsymbol{\lambda}_0)\tilde{\mathbf{i}}_s - \omega_\varepsilon \mathbf{J}\boldsymbol{\psi}_{s0} \tag{3.51a}$$

$$\tilde{\mathbf{i}}_s = \mathbf{L}_s^{-1}\tilde{\boldsymbol{\psi}}_s + (\mathbf{J}\mathbf{i}_{s0} - \mathbf{L}_s^{-1}\mathbf{J}\boldsymbol{\psi}_{s0})\tilde{\theta}_m \tag{3.51b}$$

where operating-point quantities are marked by subscript 0. By substituting (3.51b) for $\tilde{\mathbf{i}}_s$ in (3.51a), the linearized system can be expressed in state-space form

$$\dot{\tilde{\boldsymbol{\psi}}}_s = \underbrace{-(R_s\mathbf{I} + \omega_{m0}\mathbf{J}\mathbf{L}_s + \boldsymbol{\lambda}_0)\mathbf{L}_s^{-1}}_{\mathbf{A}}\tilde{\boldsymbol{\psi}}_s + \underbrace{(R_s\mathbf{I} + \boldsymbol{\lambda})\mathbf{L}_s^{-1}(\mathbf{J}\boldsymbol{\psi}_{s0} - \mathbf{L}_s\mathbf{J}\mathbf{i}_{s0})}_{\mathbf{b}_\theta}\tilde{\theta}_m$$
$$\underbrace{-\mathbf{J}\boldsymbol{\psi}_{s0}}_{\mathbf{b}_\varepsilon}\omega_\varepsilon \tag{3.52a}$$

$$\tilde{\mathbf{i}}_s = \underbrace{\mathbf{L}_s^{-1}}_{\mathbf{C}}\tilde{\boldsymbol{\psi}}_s \underbrace{-\mathbf{L}_s^{-1}(\mathbf{J}\boldsymbol{\psi}_{s0} - \mathbf{L}_s\mathbf{J}\mathbf{i}_{s0})}_{\mathbf{d}_\theta}\tilde{\theta}_m \tag{3.52b}$$

where $\tilde{\theta}_m$ and ω_ε are considered as inputs. For obtaining a closed-loop system, the states of the adaptation mechanisms of the observer have to be included in the linearized a model. The closed-loop system is

$$\begin{bmatrix} \dot{\tilde{\boldsymbol{\psi}}}_s \\ \dot{\tilde{\theta}}_m \\ \dot{\tilde{\omega}}_m \\ \dot{\varepsilon} \\ \dot{\omega}_\varepsilon \end{bmatrix} = \begin{bmatrix} \mathbf{A} & \mathbf{b}_\theta & \mathbf{0} & \mathbf{0} & \mathbf{b}_\varepsilon \\ \mathbf{0} & 0 & 1 & 0 & 0 \\ \mathbf{k}_p\mathbf{C}\mathbf{A} + \mathbf{k}_i\mathbf{C} & \mathbf{k}_p\mathbf{C}\mathbf{b}_\theta + \mathbf{k}_i\mathbf{d}_\theta & \mathbf{k}_p\mathbf{d}_\theta & 0 & \mathbf{k}_p\mathbf{C}\mathbf{b}_\varepsilon \\ \mathbf{0} & 2K_\varepsilon\alpha_{lp} & 0 & -\alpha_{lp} & 0 \\ \mathbf{0} & \gamma_p 2K_\varepsilon\alpha_{lp} & 0 & \gamma_i - \gamma_p\alpha_{lp} & 0 \end{bmatrix} \begin{bmatrix} \tilde{\boldsymbol{\psi}}_s \\ \tilde{\theta}_m \\ \tilde{\omega}_m \\ \varepsilon \\ \omega_\varepsilon \end{bmatrix} \tag{3.53}$$

in state-space form.

The dynamics of the closed-loop system were investigated by examining the eigenvalues of the system matrix in (3.53). The eigenvalues are plotted in Fig. 3.5 as the operating-point speed ω_{m0} varies from -0.15 p.u. to 0.15 p.u., and the operating-point stator current $\mathbf{i}_{s0}$ corresponds to the maximum torque-per-ampere relation at the nominal torque T_N. The high-frequency signal injection is in use below the speed 0.13 p.u. The parameters of the combined observer correspond to those of Publication **III**.

When the signal injection is in use, all the poles are located in the left half-plane. The system is stable in all the operating points investigated, indicating that the hybrid observer converges. As the speed increases and the influence of the signal injection method on the rotor speed and position estimation decreases, the dominant pole moves along the real axis towards the origin. The degree of the system decreases at the speed 0.13 p.u., and that pole disappears from the actual system.

Effect of Magnetic Saturation on the Estimation

The effect of the magnetic saturation on hybrid speed and position estimation was investigated by means of computer simulations. Because significant saturation could not be detected in the experimental motor used in this study, a simple saturation model was defined for simulations. The stator inductances are modeled as functions of the flux level. The

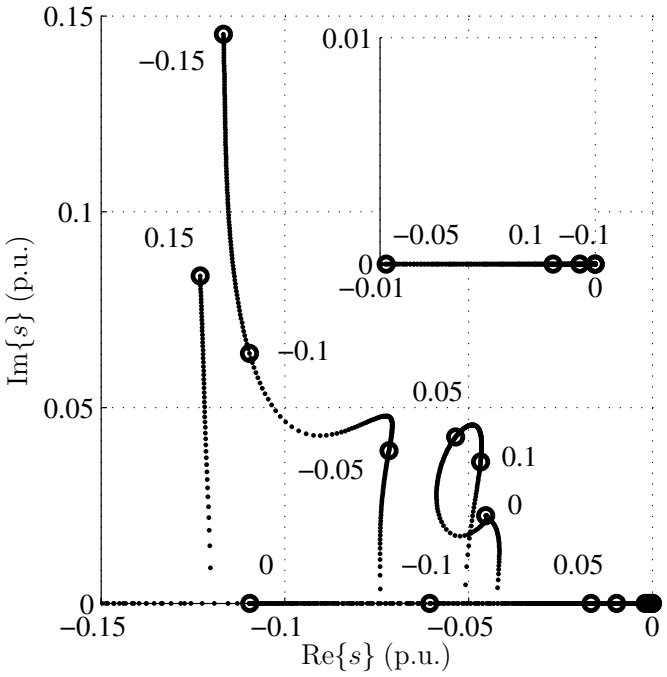

Figure 3.5: Eigenvalues of the linearized closed-loop system. The vicinity of the origin is magnified in the small subplot. The circles indicate certain values of the operating-point speed ω_{m0}.

model is based on a relation between the magnetizing current i_m and a resulting magnetic flux linkage ψ_m, (de Jong, 1980)

$$i_m(\psi_m) = \frac{1}{\alpha' L_{m0}} \left(\alpha' \psi_m + (1-\alpha') \psi_m^{a'} \right) \tag{3.54}$$

where $0 < \alpha' < 1$ and $a' > 0$ are constants and L_{m0} is the non-saturated value of the magnetizing inductance. It is to be noted that (3.54) is defined for per-unit quantities. The equation consists of a linear term and a saturated term. The magnetizing inductance can be calculated as the ratio between the resulting flux and the magnetizing current,

$$L_m(\psi_m) = \frac{L_{m0}}{1 + \alpha \psi_m^a} \tag{3.55}$$

where $\alpha = 1/\alpha' - 1 > 0$ has been introduced for convenience and $a = a' - 1$.

A model of the magnetic saturation is shown below as an example. The stator flux linkages are (Tursini et al., 2003a)

$$\psi_{sd} = L_d i_d + L_d i_f \tag{3.56a}$$

$$\psi_{sq} = L_q i_q \tag{3.56b}$$

where

$$i_f = \frac{\psi_{pm0}}{L_{d0}}$$

is an equivalent excitation current and ψ_{pm0} a non-saturated value of permanent magnet flux. The permanent magnet is thus modeled as an excitation winding having constant current. The stator inductances are defined in accordance with (3.55):

$$L_d(\psi_s) = \frac{L_{d0}}{1 + \alpha \psi_s^a}, \quad L_q(\psi_s) = \frac{L_{q0}}{1 + \beta \psi_s^b} \tag{3.57}$$

where L_{d0} and L_{q0} are non-saturated inductances and ψ_s is the stator flux amplitude.

The stator current components are

$$i_d = \frac{\psi_{sd}}{L_d(\psi_s)} - \frac{\psi_{pm0}}{L_{d0}} \tag{3.58a}$$

$$i_q = \frac{\psi_{sq}}{L_q(\psi_s)} \tag{3.58b}$$

In order for the model to be reciprocal, $\partial i_d/\partial \psi_{sq} = \partial i_q/\partial \psi_{sd}$ must apply (Melkebeek and Willems, 1990). Hence, from

$$\frac{\partial i_d}{\partial \psi_{sq}} = \alpha a \frac{\psi_{sd}}{L_{d0}} \psi_s^{a-2} \psi_{sq} \tag{3.59a}$$

$$\frac{\partial i_q}{\partial \psi_{sd}} = \beta b \frac{\psi_{sq}}{L_{q0}} \psi_s^{b-2} \psi_{sd} \tag{3.59b}$$

the relation

$$\alpha a \frac{1}{L_{d0}} \psi_s^a = \beta b \frac{1}{L_{q0}} \psi_s^b \tag{3.60}$$

is obtained, giving conditions

$$a = b, \quad \beta = \frac{L_{q0}}{L_{d0}} \alpha \tag{3.61}$$

for the saturation parameters.

Figure 3.6 shows the stator inductances and the stator flux linkage components as functions of the current components when $\alpha = 0.4$, $a = 5$, $\beta \approx 0.63$, $b = 5$, $0.56 \leq \psi_{sd} \leq 1.03$ p.u., and $0 \leq \psi_{sq} \leq 0.71$ p.u. The other parameters of the motor model correspond to those of the experimental motor defined in Chapter 4. The non-saturated values of the stator inductances and permanent magnet flux were adjusted so that they equal their nominal values in the nominal operating point. It can be seen in the figure that the inductances decrease significantly as the flux increases, and the cross-saturation effect is also visible. The saturation effect is more pronounced on the q axis than on the d axis.

The effect of the magnetic saturation described above was studied by means of simulations using load torque ramps. The speed and position estimation method used in the simulations was the adaptive observer combined with the alternating high-frequency signal injection method. The parameters of the combined observer correspond to those of Publication **III**. Fig. 3.7 shows simulation results when the speed reference is changed stepwise from zero to 0.2 p.u. at $t = 0.2$ s. The load torque is first changed stepwise from zero to T_N at $t = 0.4$ s and then ramped from T_N to $-T_N$ between $t = 1$ s and $t = 3$ s. Only the adaptive observer is used for the estimation at $\omega_m = 0.2$ p.u. The magnetic saturation is modeled in the PMSM model, but it is not taken into account in the observer. The stator inductances change approximately 3 % and 4 % on the d and q axes, respectively, which results in a small steady-state error in the estimated rotor position. It is to be noted that a steady-state position estimation error also results without load torque. This is due to the error in the estimated permanent magnet flux: the permanent magnet flux changes with stator current when the saturation is modeled in the permanent magnet machine.

Fig. 3.8 shows simulation results corresponding to the simulation in Fig. 3.7, but the magnetic saturation has been taken into account in the adaptive observer and in the current controller. Because the saturation models are equal in the observer and in the simulation model of the motor, the estimated stator inductances are close to those of the motor model.

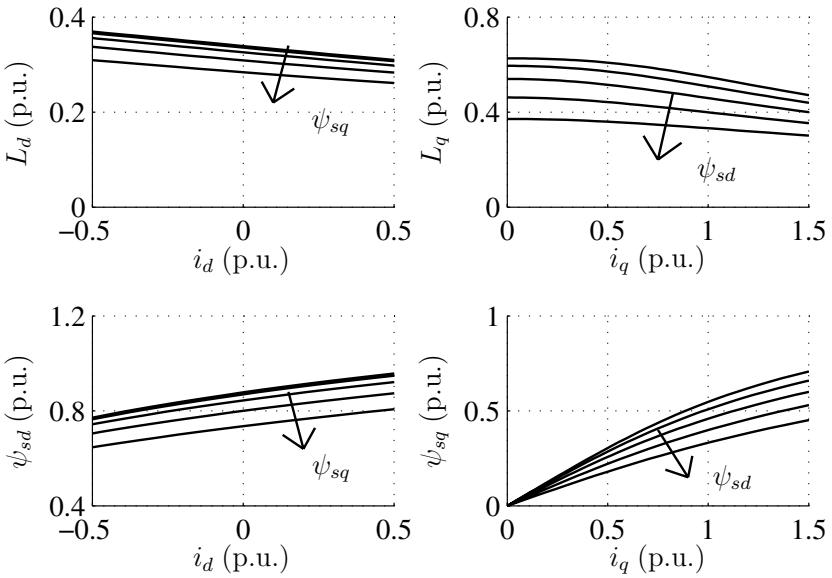

Figure 3.6: Modeled inductances and stator flux linkages as functions of the stator currents. The arrows indicate increasing flux linkages.

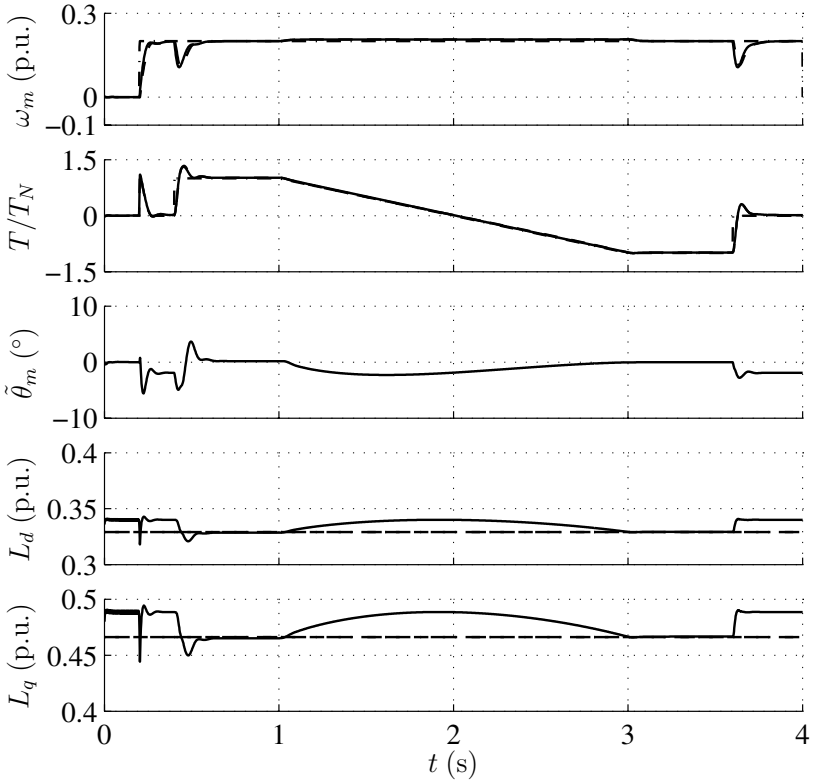

Figure 3.7: Simulation with constant inductances in the adaptive observer. First subplot shows electrical angular speed (solid), its estimate (dashed), and its reference (dash-dotted). Second subplot shows electromagnetic torque (solid), its estimate (dashed), and load torque (dash-dotted). Third subplot shows estimation error of the rotor position. Fourth subplot shows stator inductance d-component (solid), its estimate (dashed), and its nominal value (dash-dotted), and last subplot corresponding quantities for stator inductance q-component.

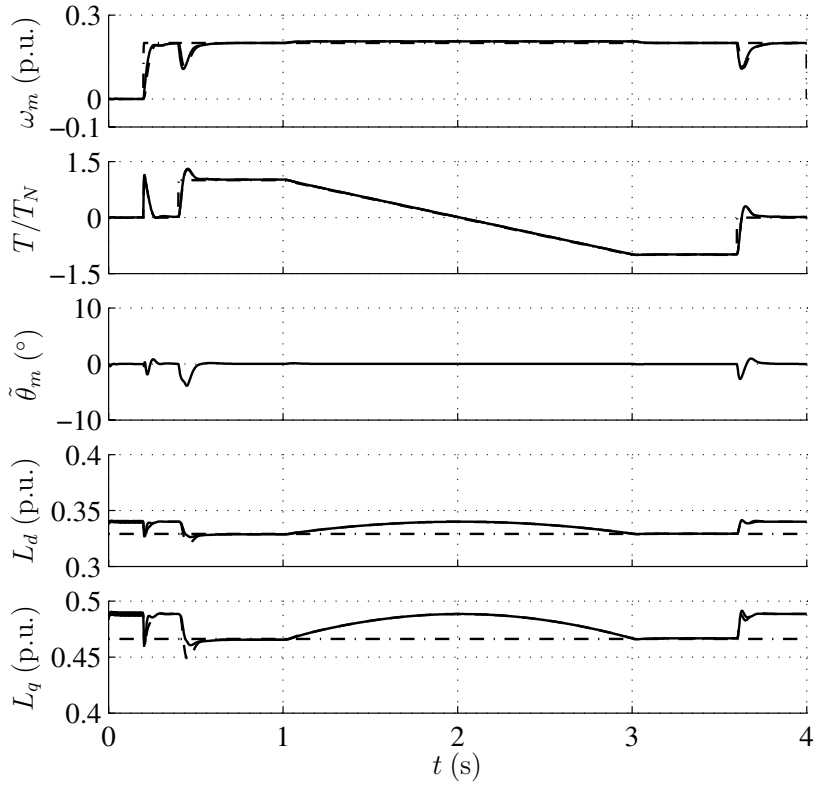

Figure 3.8: Simulation with saturation model included in the adaptive observer. Explanations of the curves are as in Figure 3.7.

Consequently, the rotor position estimation error reduces to a negligible value in steady state.

The effect of the saturation on the signal injection method was investigated by load torque ramps at low speeds. Fig. 3.9 shows simulation results at zero speed reference when the load torque was changed stepwise from zero to T_N at $t = 0.4$ s and then ramped to $-T_N$ between $t = 1$ s and $t = 3$ s. A model for the magnetic saturation is included in the motor model, and the saturation is taken into account in the estimated inductances. According to the results, a significant error appears in the estimated position. Because the stator inductances are inaccurately estimated due to the position estimation error, the saturation model in the observer even impairs the performance. It can thus be concluded that the signal injection method is strongly affected by the magnetic saturation. The magnetic anisotropy is shifted due to the cross-saturation effect, and the estimated rotor position converges to an erroneous value.

For the compensation of saturation effects, the method proposed by Li et al. (2007) was employed. The idea of the method is to use the current

$$i_{cd} = i'_d + \gamma i'_q \tag{3.62}$$

for demodulation in (3.36) instead of using only the current component i'_q. In (3.62), γ is a parameter that can be chosen by means of finite-element analysis or experimentally (Li et al., 2007).

For obtaining γ, a simulation was performed using only the adaptive observer for the estimation. In steady state, the current i_{cd} of (3.62) is driven to zero, and it is thus required

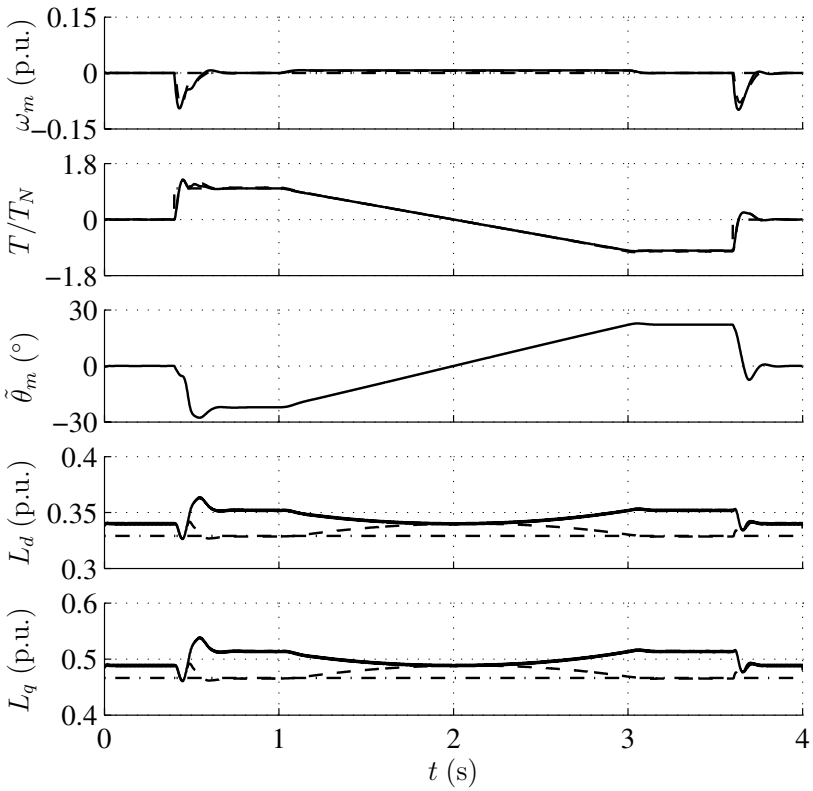

Figure 3.9: Simulation results with saturation model included in the adaptive observer and original signal injection method. Explanations of the curves are as in Figure 3.7.

that

$$\gamma = -\frac{i'_d}{i'_q} \tag{3.63}$$

Fig. 3.10 shows simulation results corresponding to the simulation in Fig. 3.7. A model for the saturation is included both in the motor and in the adaptive observer. The signal injection is in use for obtaining the high-frequency current components i'_d and i'_q, but it is not used for the estimation. It can be seen that the parameter γ is almost proportional to the q component of the stator current, which has the most significant contribution to the electromagnetic torque. According to the simulation of Fig. 3.10, $\gamma \approx -0.22 i_{q0}$ in per units, i_{q0} being the operating-point q component of the stator current.

A new simulation corresponding to that of Fig. 3.9 was performed with the modified signal injection method. The results shown in Fig. 3.11 indicate that the method proposed by Li et al. is effective. The rotor position estimation error is small, and the performance is greatly improved.

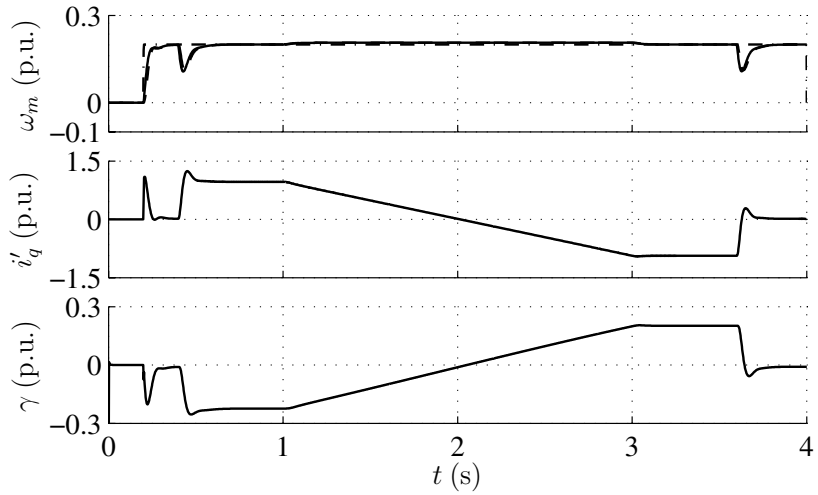

Figure 3.10: Simulation results for determining parameter γ. First subplot shows electrical angular speed (solid), its estimate (dashed), and its reference (dash-dotted). Second subplot shows stator q-axis current in estimated rotor reference frame. Third subplot shows the correction parameter of the signal injection method.

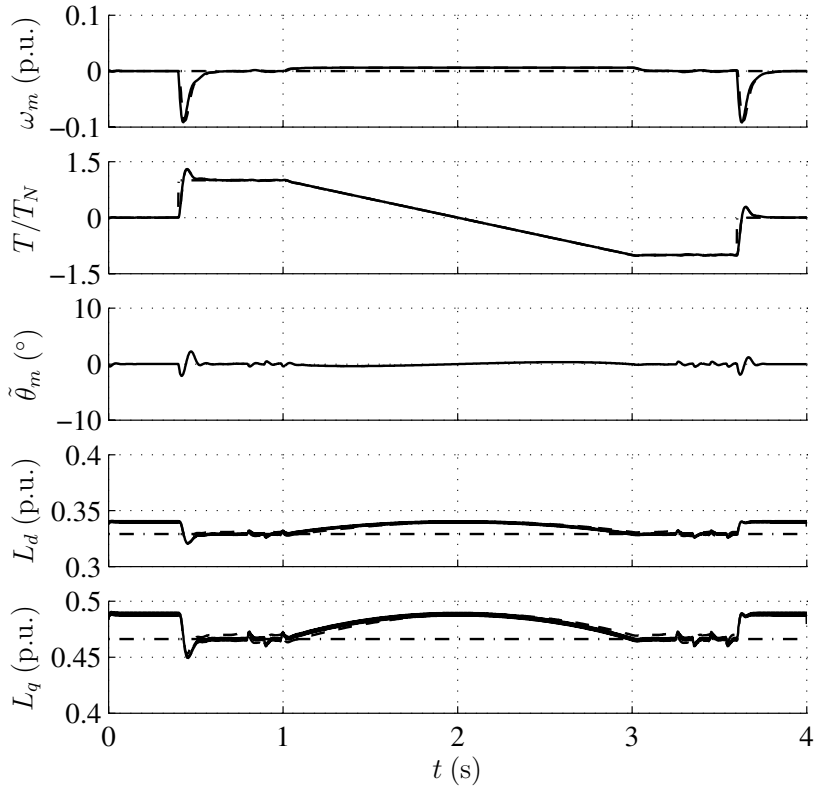

Figure 3.11: Simulation results with saturation model included in the adaptive observer and modified signal injection method. Explanations of the curves are as in Figure 3.7.

3.4 Effect of Parameter Errors and Parameter Adaptation

The fundamental-excitation methods need the electrical parameters for the estimation. Omitting the spatial harmonics, the required parameters are the stator resistance R_s, the stator d- and q-axis inductances L_d and L_q, respectively, and the permanent magnet flux ψ_{pm}. If the parameters are not known, they have to be identified prior to normal operation.

The motor parameters vary depending on the operating conditions, and the accuracy of the estimates is thus not always sufficient. The incorrect parameter estimates degrade the performance of the current control and the speed and position estimation. The stator resistance and the permanent magnet flux depend on the motor temperature; the stator resistance increases while the permanent magnet flux decreases as the PMSM warms up. On the other hand, the stator inductances are affected by the magnetic saturation. If good performance is demanded as the parameters change, variable parameter estimates are necessary. The stator inductance components can be modeled as functions of the stator current or the stator flux, but the stator resistance and permanent magnet flux estimates need to be estimated on-line as the drive operates.

Kim et al. (1995) proposed the use of adaptation mechanisms for estimating the motor parameters in a PMSM drive equipped with a motion sensor. The components of the current estimation error were used for the adaptation of the stator resistance and the permanent magnet flux. Of particular importance, if additional excitation signals are not used, the two degrees of freedom of the PMSM dynamics permit the estimation of only two quantities, which include the rotor speed. The method used by Kim et al. (1995) is in line with this limitation. Conversely, Ichikawa et al. (2006) used a recursive method for estimating three quantities, the stator resistance and both the stator d- and q-axis inductances in sensorless control. According to the experimental results, at least the stator resistance estimate varies in a way that cannot be explained by thermal changes. The convergence of the parameter adaptation was not shown by simulations.

In Publication **IX**, a method for the adaptation of the stator resistance and the permanent magnet flux is added to the combined observer of Fig. 3.4. The idea is to exploit the additional information in the observer that is not used for sensorless control. The d component of the current estimation error and the speed correction term ω_ε depend on the parameter errors, and the estimated parameters can be adjusted such that $\tilde{i}_d$ and ω_ε are driven to zero. At medium and high speeds, the permanent magnet flux is estimated from $\tilde{i}_d$, whereas at low speeds, the stator resistance is estimated using ω_ε. The developed method is illustrated in Fig. 3.12.

It is shown experimentally in Publication **IX** that the proposed parameter adaptation improves the overall performance of the drive. As a drawback, the proposed method cannot distinguish between the errors in the permanent magnet flux ψ_{pm} in the stator inductance d component at medium and high speeds. However, the inductances do not depend on the temperature, and their dependence on magnetic saturation can be modeled separately.

3.5 Cascaded Speed and Current Control

The block diagram of the control system for a motion-sensorless PMSM drive is shown in Fig. 3.13. Cascade control is used to control the rotor speed and the stator current. The speed controller provides the electromagnetic torque reference. The stator current ref-

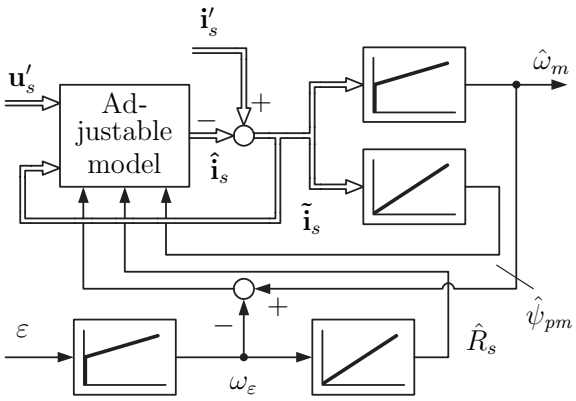

Figure 3.12: Combined observer with parameter adaptation.

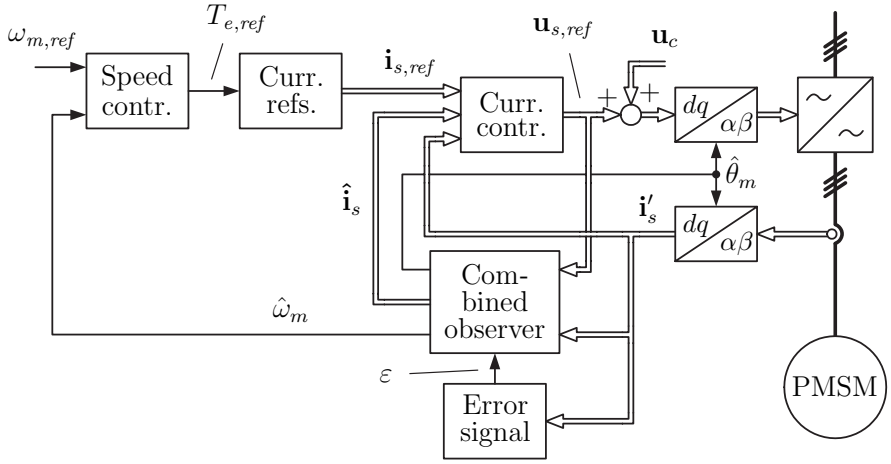

Figure 3.13: Block diagram of the control system comprising cascaded speed and current control loops. Vector quantities on the left-hand side of coordinate transformations are in the estimated rotor reference frame and on the right-hand side in the stator reference frame.

erence $\mathbf{i}_{s,ref}$ is calculated according to the maximum torque-per-ampere relation (Jahns et al., 1986) from the torque reference. The current components are controlled by PI controllers, and feedforward compensation is applied for the cross-coupling terms and the back-emf (Briz del Blanco et al., 1999). The rotor speed is governed by an IP-type speed controller.

In Publications **I–III**, predicted stator current is used for feedback in the proportional part of the current controller. The current prediction is based on the dynamic model of the motor (Springob and Holtz, 1998). The estimated stator current is used for feedback in the proportional part of the current controller in Publications **IV**, **V**, and **IX**. Since the estimated stator current is also based on the dynamic motor model, it principally behaves like the predicted current in transients. The estimated current can have a larger steady-state error, but is not as sensitive to the system noise as the predicted current.

3.6 Torque Ripple Compensation

The spatial harmonics in the PMSM described in Chapter 2 cause load-dependent harmonics in the electromagnetic torque if conventional current control is used. In addition, the stator slots can cause cogging torque that is independent of the stator current. The torsional

vibrations caused by these phenomena degrade the performance of the PMSM drive. The vibrations can excite mechanical resonances, leave patterns to workpieces if the drive is used for machining, or they can sometimes be heard as audible noise.

Several methods have been presented to mitigate the torque ripple. Mostly, the methods deal with surface-magnet machines that are non-salient. In addition to the cogging torque, the primary source of the ripple in the surface-magnet machines is usually the harmonics in the permanent magnet flux. The electromagnetic torque recalled from (2.30) is

$$\begin{aligned} T_e = \frac{3p}{2}\big\{ & \psi_{pm0} i_q + (L_d - L_q) i_d i_q \\ & - 2L_6 \sin(6\theta_m)(i_d^2 - i_q^2) - 4L_6 \cos(6\theta_m) i_d i_q \\ & + i_q \cos(6\theta_m)(\psi_{d6} + 6\psi_{q6}) - i_d \sin(6\theta_m)(\psi_{q6} + 6\psi_{d6}) \big\} \end{aligned} \tag{3.64}$$

For the surface-magnet machines, $L_d = L_q$ is assumed, and the current component i_d is usually controlled to zero. The inductance harmonics as the source of the torque ripple are omitted in many cases (Chung et al., 1998). Hence, (3.64) is reduced to

$$T_e = \frac{3p}{2} i_q \big\{ \psi_{pm0} + \cos(6\theta_m)(\psi_{d6} + 6\psi_{q6}) \big\} \tag{3.65}$$

It is relatively simple to determine i_q from T_e using (3.65). Direct calculation of the current reference i_q was used by Wu and Chapman (2005).

Contrary to the surface-magnet machines, Madani et al. (1995) stated that the inductance harmonics is the most significant source of the torque ripple in salient machines. It is obvious that optimal current references cannot be solved easily from (3.64) in the presence of L_6 if i_d is nonzero. The determination of the current references i_d and i_q that would lead to constant torque is a difficult optimization procedure (Madani et al., 1995). Therefore, a method where an on-line controller is used for suppressing the torque harmonics could be a feasible solution. Low et al. (1990) and Colamartino et al. (1999) have proposed the use of on-line controllers, but these methods do not exploit the reluctance torque, which leads to a weakened torque-to-current ratio.

Publication **V** of this thesis deals with the torque ripple reduction in salient PMSMs. The method is based on controlling the harmonics in the estimated electromagnetic torque to zero. The current references are controlled such that the current trajectory varies along the maximum torque-per-ampere curve. Compared to the previous methods, this method has the following advantages:

- It takes into account harmonics both in the permanent magnet flux and in the stator inductance
- The reluctance torque is used for a better torque-to-current ratio
- The method is applicable to sensorless drives

For the reduction of the electromagnetic torque ripple, an additional block is added to the control system, resulting in the system shown in Fig. 3.14. The harmonic components of the torque are estimated using the measured stator current and the estimated rotor position. A feedback term is subtracted from the fundamental torque reference $T_{ref,0}$ in order to suppress the specified harmonics in the estimated torque. For the tracking of the harmonic current references, the current controller is augmented with PI-controllers in reference frames rotating at the frequency of the harmonics both in the positive and negative directions (Song and Nam, 1999).

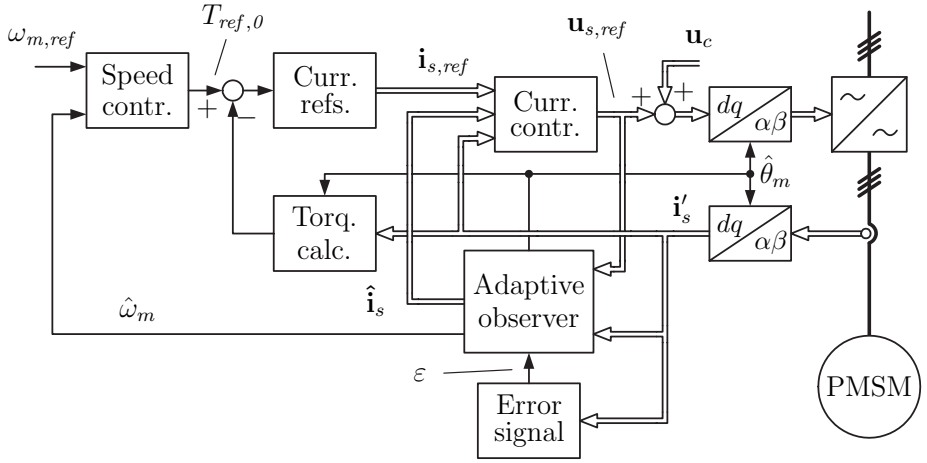

Figure 3.14: Block diagram of the control system with torque ripple compensation. The block "Torq. calc." includes the algorithm for the suppression of the torque harmonics. The current controller is augmented with control of the harmonic components.

Experiments on the Torque Ripple Compensation

Torque measurements were not possible in Publications **IV** and **V**. Shaft torque measurements were performed later in order to investigate the effectiveness of the proposed methods. It is worth noticing that the shaft torque differs from the electromagnetic torque because of friction and windage losses and the inertia of the PMSM. In the experimental system, the moment of inertia of the PMSM is larger than the inertia of the servo motor used as the load machine. Furthermore, the unknown torque ripple generated by the load machine also contributes to the shaft torque.

To investigate the effect of the method of Publication **V** on the torque ripple, the shaft torque was measured by using a torque sensor. Figure 3.15 shows the harmonic components T_k of the torque when the drive operated in steady state at $\omega_m = 0.5$ p.u. and $T_l = T_N$. The harmonic components were calculated off-line from the captured measurement data using Fourier analysis. According to the results, the sixth harmonic is the most significant harmonic component of the torque, being almost 1 % of the average torque. The proposed method for the torque ripple suppression reduces the sixth harmonic of the torque by 53 %.

Measured steady-state values of the sixth harmonic component of the torque (as percentage of the average torque) are listed in Table 3.1 in different operating points. In all

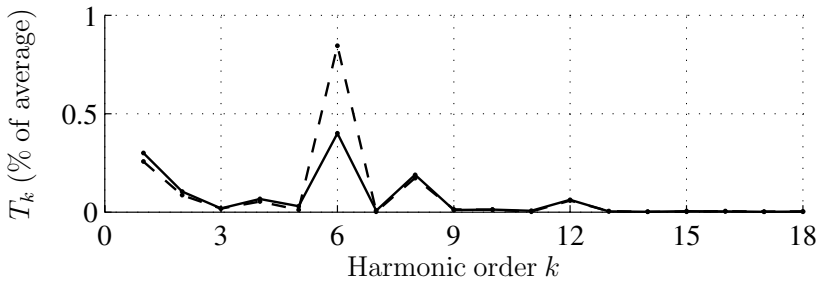

Figure 3.15: Measured harmonic components of the shaft torque in % of the average torque when $\omega_m = 0.5$ p.u. and $T_l = T_N$. Dashed line shows the components obtained with the original method, and solid line with the proposed method.

Table 3.1: Measured sixth harmonic of shaft torque in different operating points

ω_m (p.u.)	Operating mode	T_l/T_N	Sixth harmonic of torque, % of average		Change in %
			Original	Proposed	
0.2	Motoring	1.0	1.05	0.63	−39.9
0.2	Motoring	0.5	1.09	0.68	−38.4
0.2	Regenerating	−0.5	0.85	0.67	−20.3
0.2	Regenerating	−1.0	0.98	0.93	−5.1
0.5	Motoring	1.0	0.85	0.40	−52.7
0.5	Motoring	0.5	0.88	0.53	−40.4
0.5	Regenerating	−0.5	0.60	0.13	−78.2
0.5	Regenerating	−1.0	0.66	0.44	−34.2
0.67	Motoring	1.0	1.23	0.73	−41.1
0.67	Motoring	0.5	1.64	0.90	−45.1
0.67	Regenerating	−0.5	1.07	0.14	−86.8
0.67	Regenerating	−1.0	1.11	0.71	−35.8

operating points, the proposed method decreases the sixth harmonic of the torque. The reduction is not significant at low speed in the regenerating mode, where the stator voltage is small and the inverter nonlinearities have a bigger effect on the estimation.

Although the reduction in the sixth harmonic of the estimated torque is more than 99 % in all operating points investigated, the reduction of the sixth harmonic in the measured torque is less remarkable. Hence, good accuracy of the torque ripple estimation is an essential part of the proposed algorithm. A good performance of the position estimation is also required, because the position estimate is needed in the torque calculation according to (3.64).

3.7 Sensorless Control With Inverter Output Filter

The PMSMs are usually fed by pulsewidth-modulated inverters. The high-frequency harmonics of the inverter output voltage cause additional losses and audible noise. The high rate of change of the voltage causes stresses in the stator winding insulations, and the common-mode leakage currents through the parasitic capacitances of the stator windings can cause bearing currents. An inverter output filter can be used to overcome these problems. A du/dt filter reduces the high-frequency phenomena, but if the target is to reduce the additional losses in the motor and acoustic noise, a sinusoidal filter having a cut-off frequency below the switching frequency has to be used.

An LC filter is a commonly used topology for a sinusoidal filter. The drawback of the filter is that it complicates the control of the drive since the motor voltages and currents differ from those of the inverter output. Feedforward compensation can be used to reduce the effects of the filter on the current control (Carpita et al., 1991). A more precise control of the stator current is possible if cascaded control is used, but it requires knowledge of the motor voltage and current. Zimmermann (1988) used cascaded control in induction motor drives with direct measurement of the stator voltage and current, while Salomäki et al. (2006) used an adaptive full-order observer for the estimation of the motor-side quantities in a sensorless induction motor drive. By estimating the stator voltage and current instead of direct measurements, the costs can be reduced and the filter can be added to an existing

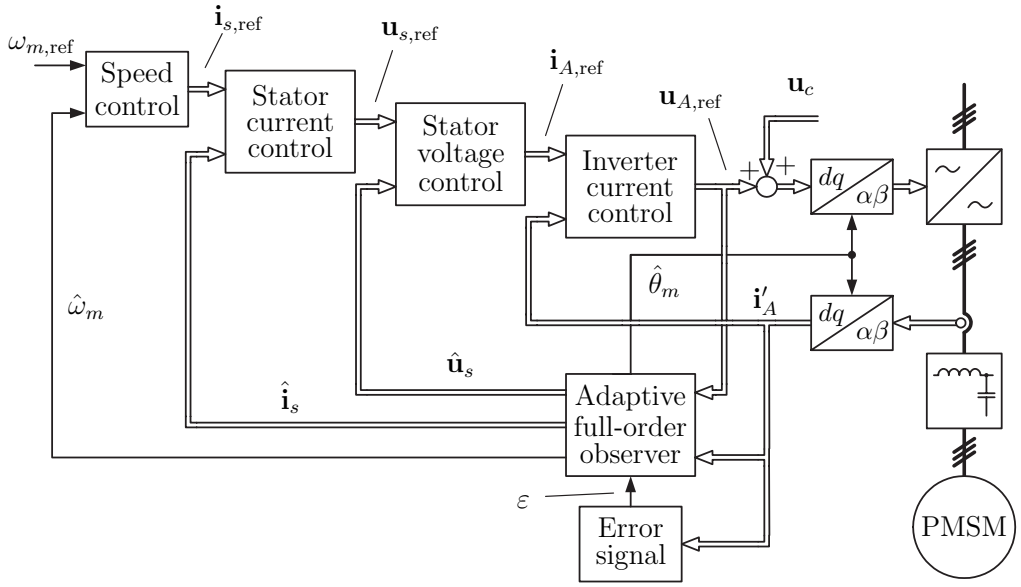

Figure 3.16: Block diagram of the control system for PMSM drive equipped with inverter output LC filter. The speed control includes the calculation of the stator current reference according to the maximum torque-per-ampere method.

drive by modifying only the control software.

A method similar to the one introduced by Salomäki et al. is proposed in Publication **VI** of this thesis for sensorless PMSM drives. An adaptive full-order observer is used for the estimation of the stator voltage, the stator current, and the speed and position of the PMSM. Cascaded control is used for controlling the rotor speed, the stator current, the stator voltage, and the inverter current. In Publication **VII**, the HF signal injection is investigated in a PMSM drive equipped with an LC filter, and the adaptive full-order observer is augmented with the alternating signal injection method at low speeds. The HF signal injection enables sensorless operation of the drive at low speeds and down to zero speed.

It was found out that with proper selection of the injection frequency, the inverter output filter actually increases the sensitivity of the system to the HF excitation signal. However, the increased sensitivity does not necessarily lead to improved performance. It is preferable that the current resulting from the HF excitation is small. Due to the increased sensitivity, the excitation voltage may need to be reduced, which in turn increases the voltage error caused by inverter nonlinearities. In the case of Publication **VII**, the increase in the gain is negligibly small, and the performance is comparable to the case without the filter.

Fig. 3.16 shows a block diagram of the control system for a motion-sensorless PMSM drive including the inverter output LC filter. The system according to Fig. 3.16 is used in Publications **VI** and **VII**. The speed controller and the calculation of the current reference correspond to that of the control system without the filter. Two additional control loops are added inside the stator current control loop: stator voltage control and inverter current control. The bandwidth of the inner control loop is higher than that of the outer control loop. In the proportional part of the inverter current controller, predicted inverter current is used for feedback (Springob and Holtz, 1998). The stator voltage and stator current controllers use estimated quantities for feedback, because the actual quantities are not measured.

3.8 DC-link Current Measurement

The stator current vector control requires feedback from the motor phase currents. The current feedback is usually obtained using direct measurement of at least two phase currents. In low-cost frequency converters, the current sensors used for measuring the currents form a substantial part of the manufacturing cost. In addition, the properties of the current sensors in different inverter output phases may be different. The deviation between the sensor gains impairs the accuracy of the current control, and even causes torque ripple.

An alternative to the phase current measurement is to measure the DC-link current of the inverter. The DC-link current sensor does not require electrical isolation from the control electronics, and can thus be realized using a shunt resistor. In contrast to the phase current measurement, the DC-link current measurement can also be used for supervising the fault current during possible inverter shoot-through. The phase currents required for the vector control can be deduced from the DC-link current and the information on the states of the inverter switches (Green and Williams, 1989); the DC-link current equals one of the inverter output phase currents during nonzero inverter output voltage.

Several methods related to inverter DC-link current measurement have been proposed. Since the DC-link current is zero during zero inverter output voltage, a simple alternative is to prevent the use of zero voltage as proposed by Habetler and Divan (1991). The method proposed by Kobayashi et al. (2006) uses SVPWM with carrier signals shifted by 120° between phases. This approach also leads to exclusively nonzero inverter voltage at zero voltage reference. The nonzero inverter output voltage results in remarkably increased switching-frequency current ripple, noise, and additional losses. Kim and Jahns (2006) used a sequence of active voltage vectors for the sampling of all three phase currents. This method has the drawback that the normal operation of the inverter has to be interrupted during the measurement sequence. The method proposed by Blaabjerg et al. (1997) is based on measurements during normal PWM operation. However, the method requires four current samples in each modulation period. In addition, the sampling instants vary depending on the PWM pulse pattern.

Moynihan et al. (1993) used a state observer with a PMSM drive equipped with DC-link current measurement. The estimated stator current provided by the state observer is updated completely or partially once during switching period, depending on whether one or two phase currents are sampled. Since the PMSM can be modeled with sufficient accuracy, it is sensible to use the motor model in determining the phase currents as was done by Moynihan et al. The method proposed in Publication **VIII** of this thesis is also based on the motor model through the use of the adaptive observer. Instead of directly updating the estimated phase currents, the current feedback is based on the current estimation error.

The block diagram in Fig. 3.17 illustrates the system proposed in Publication **VIII**. A two-phase PWM method is used where the nonzero inverter output voltage is applied either at the beginning or at the center of the switching period. The DC-link current is sampled once in the switching period during nonzero inverter output voltage. The current estimation error is updated based on the available current samples and the known switching states $\mathbf{h}_{abc}$ of the inverter. At low-speeds, the position estimation is augmented with the alternating HF signal injection method, and a modified excitation voltage signal is used. In contrast to the methods in the other publications of the thesis, the HF excitation voltage is included in the voltage reference fed to the adaptive observer for the estimation of the HF current. The reconstructed stator current $\mathbf{i}_{s,dc} = \hat{\mathbf{i}}_s + \tilde{\mathbf{i}}_s$ is used for demodulation in the signal injection method.

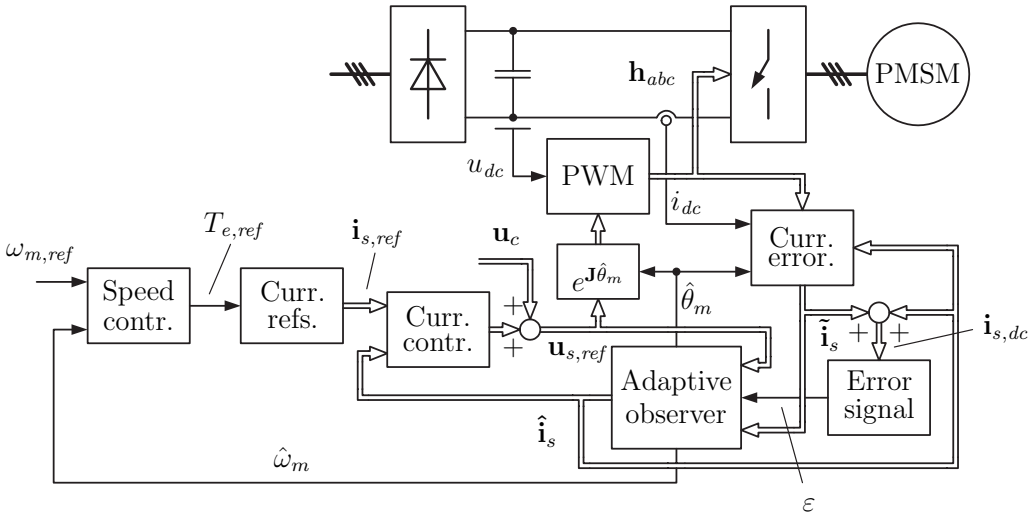

Figure 3.17: Block diagram of the control system with DC-link current measurement.

Chapter 4

Experimental Setup

The laboratory setup used in the experiments of Publications **I**-**VII** and **IX** is shown in Fig. 4.1. In Publications **VI** and **VII**, an LC filter was added between the inverter and the PMSM. In Publication **IX**, additional 1-Ω resistors were added in series to the output of the frequency converter supplying the PMSM. A manually-operated three-phase switch was connected in parallel with the resistors to enable stepwise changes in the resistance of the system. The technical data of the hardware used in the laboratory experiments is listed in Table 4.1. The permanent magnet motor is an experimental interior-magnet motor. The stator is taken from a commercial induction machine, and the permanent magnets are buried inside the rotor. The three-phase stator winding is delta-connected. The parameters of the PMSM are given in Table 4.2, and the parameters of the inverter output filter used in Publications **VI** and **VII** in Table 4.3. The permanent-magnet servomotor is fed by a commercial ABB Bivector frequency converter.

In the laboratory tests of Publications **I**-**VII** and **IX**, the PMSM is fed by a Danfoss VLT5004 frequency converter that has modified control electronics: the original control board is replaced by an interface card made at Aalborg University in Denmark (Teodorescu et al., 2000). The control algorithms are implemented using the MATLAB/Simulink environment. A part of the algorithms are written in C language and compiled for use with

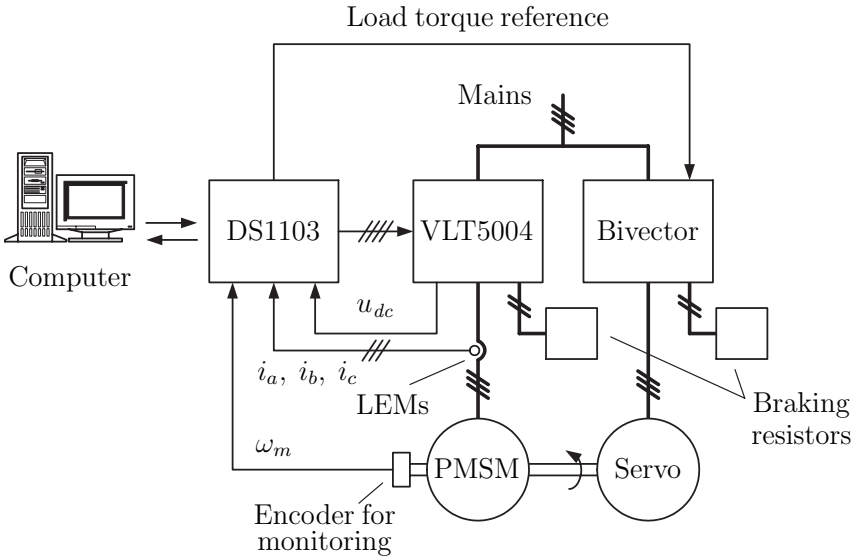

Figure 4.1: Block diagram of the experimental setup used in the laboratory tests with inverter output phase current measurement.

Table 4.1: Technical data of laboratory hardware. Current and voltage values are rms values. Three-phase voltages are phase-to-phase voltages.

PMSM	ABB M2BJ 100L 6 B3
Rating plate	370 V, 4.3 A, 75 Hz
	1 500 r/min, 2.2 kW, $\cos\varphi = 0.90$
Freq. converter for PMSM used in Publications I-VII and IX	
Model	Danfoss VLT5004 P T5 B20 EB R3 (modified)
Supply voltage	380...500 V (50/60 Hz)
Output voltage	0...100 % of supply voltage
Max. const. output current	5.6 A
Output frequency	0...1 000 Hz
Freq. converter for PMSM used in Publication VIII	
Model	ABB ACS350-03E-05A6-4
	(modified software)
Rated output power	2.2 kW
Supply voltage	380...480 V (48...63 Hz)
Output voltage	0...100 % of supply voltage
Max. input current	9.6 A
Max. const. output current	5.6 A
Output frequency	0...500 Hz
Inverter Output Filter used in Publications VI and VII	
3-phase inductor	Block B0403092 3 LC Filter for ABB
	VFD ACS 800 Series (capacitors removed)
Inductance	3 x 5.10 mH
Voltage range	0...440/520 V
Frequency range	0...150 Hz
Rated current	10.0 A
Capacitor	3 x EPCOS B25834-L6685-K009 MKV
Capacitance	6.8 µF $\pm$10 %
Rated voltage	900 V
PM servo motor	ABB 8C5 230 00YA02SL3MB
Rating plate	315 V, 3 000 r/min,
	cont. stall torque 21.5 Nm (14.1 A),
	peak stall torque 75.3 Nm (54.6 A)
Freq. converter for PM servo	ABB Bivector 535 "25"
Rated supply voltage	400 V (50/60 Hz)
Rated output voltage	400 V
Rated cont. output current	25.0 A
Current transducers	LEM LA 55-P/SP1
Bandwidth	0...200 kHz (-1 dB)
Accuracy (at 25°C, rated current)	$\pm$0.9 %
Incremental encoder	Leine & Linde 861007976
Line counts	2 048 ppr
Controller board	dSPACE DS1103 PPC
Master processor	PowerPC 604e (400 MHz, 2 MB local
	SRAM, 128 MB global DRAM)
Slave processor	Texas Instruments TMS320F240 DSP
	(20 MHz, 3-phase PWM generation)

Table 4.2: Parameters of the interior permanent magnet motor used in the laboratory tests.

Nominal torque T_N	14.0 Nm
Number of pole pairs p	3
Stator resistance R_s	3.59 Ω
Direct-axis inductance L_d	0.036 H
Quadrature-axis inductance L_q	0.051 H
Inductance 6th harmonic amplitude L_6	1.1 mH
Permanent magnet flux ψ_{pm0}	0.545 Vs
Flux harmonic amplitude ψ_{d6}	-1.0 mVs
Flux harmonic amplitude ψ_{q6}	1.4 mVs
Total moment of inertia	0.015 kgm^2

Table 4.3: Parameters of the inverter output filter used Publications **VI** and **VII**

Inductance L_f	5.1 mH
Capacitance C_f	6.8 μF
Inductor series resistance R_{Lf}	0.1 Ω

Simulink. The Simulink model includes interface blocks for the use with the dSPACE DS1103 processor board. The Simulink model is compiled for real-time execution, and the compiled software is uploaded into the DS1103 board. The DS1103 board runs two processors simultaneously. A PowerPC 604e RISC processor acts as a master processor and includes the developed control algorithms. A Texas Instruments TMS320F240 DSP acts as a slave processor, and it includes a built-in pulsewidth modulator for creating the control signals for the inverter switches.

The DS1103 board has a bundle of digital and analogue connections, through which the board is linked to a signal conditioning unit (SCU) that is made at Aalborg University. The SCU serves as an interface between the DS1103 and the other hardware in the system. The SCU feeds four control signals to the interface card on the VLT5004. Three of these control signals are the switching functions for the inverter output phases, and one is for the braking chopper. The interface includes a fixed dead time generation of 1.5 µs for the control of the inverter upper and lower branches. Other connections of the SCU include the analogue load torque reference fed to the Bivector servo drive, the measurement of the DC-link voltage of VLT5004 through the interface card attached to it, and a connection to an incremental encoder mounted on the shaft of the PMSM. The output phase currents of VLT5004 are fed through LEM's current transducers, whose outputs are connected to the SCU. A picture of the laboratory setup used with the phase current measurement is shown in Fig. 4.2.

Fig. 4.3 shows the laboratory setup used in the experiments of Publication **VIII**. The PMSM is fed by a commercial ABB ACS350 frequency converter, whose software was modified in this research. The converter has measurements only from the DC-link voltage and current; the inverter output phase currents are not measured. The converter has a Texas Instruments TMS320F2811 DSP, and the control algorithms are implemented in C language. The ACS350 was connected to the computer through a serial link having a data transfer rate of 115.2 kbps. The dSpace DS1103 board was used in the experiments for monitoring the actual speed and position of the PMSM and for the generation of the load torque reference.

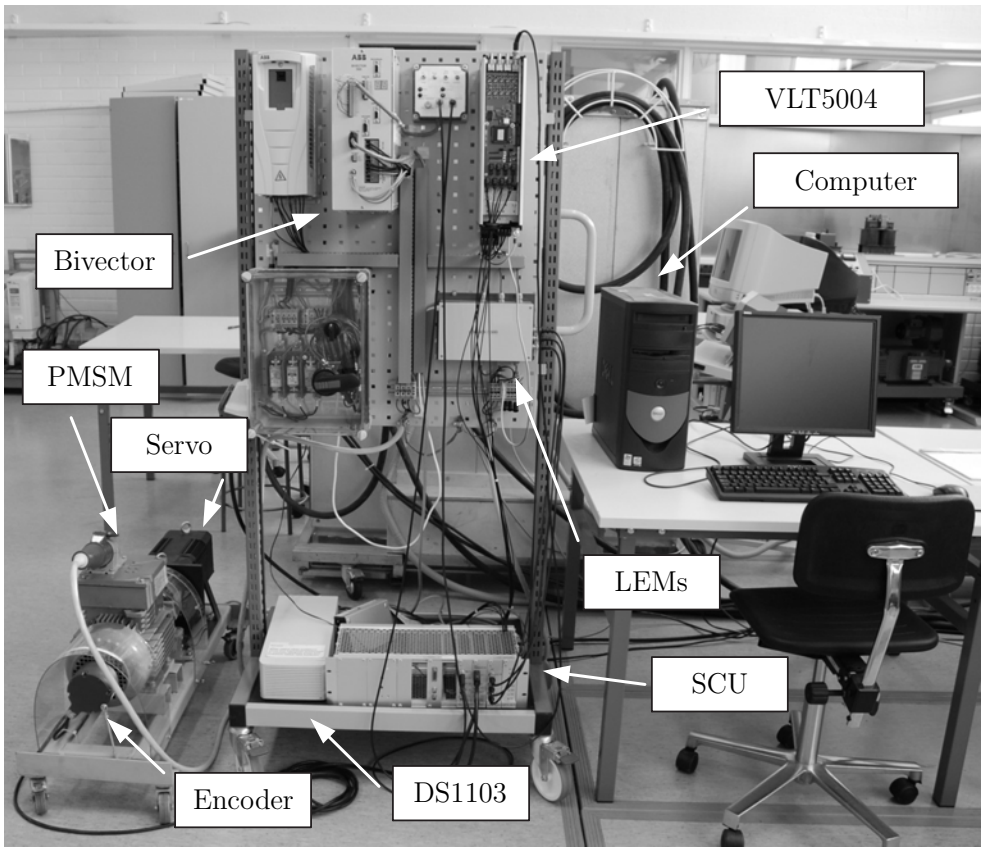

Figure 4.2: Picture of the experimental setup with phase current measurement.

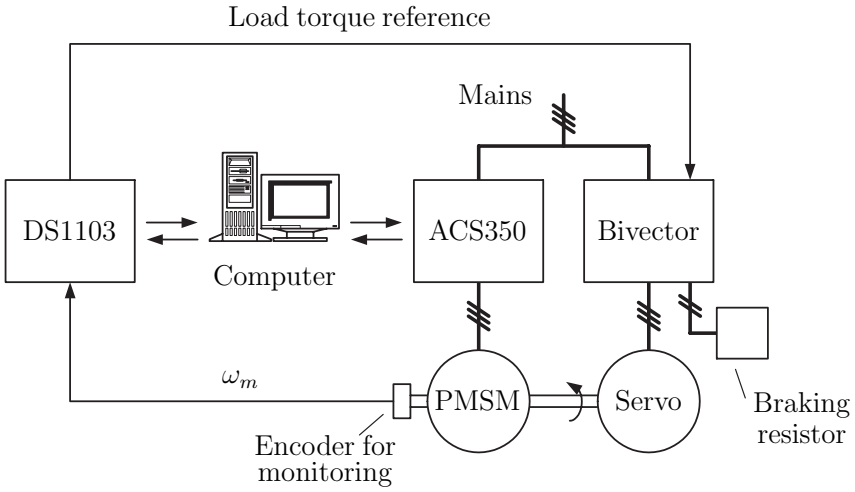

Figure 4.3: Block diagram of the experimental setup used in the laboratory tests with inverter DC-link current measurement.

Chapter 5

Summaries of Publications

The abstracts of the publications are reprinted below. Publications **I** and **II** deal with combinations of a fundamental-excitation method and a signal injection method, and Publication **III** deals with adaptive observers and their dynamic properties. Publications **IV** and **V** deal with spatial harmonics in the PMSM and reduction of their effects in motor control. Publications **VI** and **VII** deal with sensorless control as an LC filter is used at the inverter output. Publication **VIII** deals with sensorless control when only the DC-link current of the inverter is measured, and Publication **IX** deals with the adaptation of the parameters of the PMSM. The scientific contributions of the thesis are listed in Section 5.2.

5.1 Abstracts

Publication I

This paper presents a method for the rotor speed and position estimation of permanent magnet synchronous motors in a wide speed range including standstill. The proposed method is based on a modified voltage model at high speeds, and combines the modified voltage model with a high-frequency signal injection technique at low speeds. The fast dynamic response of the voltage model is thus augmented with the steady-state accuracy of the high-frequency signal injection technique. The stability and robustness of the combined observer are confirmed by simulations and experiments.

Publication II

The paper presents a speed and position estimation method for the sensorless control of permanent magnet synchronous motors. The method is based on a speed-adaptive flux observer that is augmented with a high-frequency signal injection technique at low speeds and standstill. In the adaptive observer, a flux model is used as the reference model and a voltage model as the adaptive model. At low speeds, the estimation is further corrected with an error signal from the signal injection method by influencing the direction of the estimated stator flux. The fast dynamic response of the adaptive observer is thus combined with the steady-state accuracy of the high-frequency signal-injection method. According to simulations and experiments, the proposed approach is stable and robust, and can cope with stepwise changes in the speed or position reference. The capability of rejecting load torque transients is also good.

Publication III

The paper deals with a speed and position estimation method for the sensorless control of permanent magnet synchronous motors. The method is based on a speed-adaptive observer. The dynamics of the system are analyzed by linearizing both the motor model and the observer, and the observer gain is selected to give improved damping and noise suppression. At low speeds, the observer is augmented with a signal injection technique, providing stable operation down to zero speed. The experimental results, obtained using a 2.2-kW interior magnet motor, are in agreement with the results of the analysis.

Publication IV

The paper deals with speed and position estimation of permanent magnet synchronous motors having unwanted spatial harmonics in the stator inductance and in the permanent magnet flux. The sensorless control is based on an adaptive observer that is augmented with a pulsating high-frequency signal injection technique at low speeds. The effects of harmonics on the speed and position estimation are reduced by adding harmonic models of the inductances and the flux to the adaptive observer and by modifying the injected high-frequency voltage signal based on the inductance variation. Simulations and laboratory experiments show that the estimation accuracy is improved and torque pulsations are reduced.

Publication V

The paper proposes a method for the compensation of the torque ripple that is caused by motor unidealities in sensorless permanent magnet synchronous motor drives. The sensorless control of the interior-magnet motor is based on a speed-adaptive observer augmented with a pulsating high-frequency signal injection technique at low speeds. The harmonics in the permanent magnet flux and stator inductances are taken into account in the estimation, and a torque ripple compensator is developed for suppressing the harmonics in the estimated electromagnetic torque. The high-bandwidth current control required for torque ripple reduction is based on additional PI controllers implemented in reference frames rotating at the harmonic frequencies. Simulations and laboratory experiments show the effectiveness of the proposed method.

Publication VI

The paper presents a sensorless vector control method for a permanent magnet synchronous motor when the output voltage of the PWM inverter is filtered by an LC filter. The dynamics of the LC filter are taken into account in the design of the controller and adaptive full-order observer. The use of the output filter does not require additional current or voltage measurements. The speed adaptation is based on the estimation error of the inverter output current. Linearization analysis is used to design an observer that enables a wide operation region. Simulation and experimental results show the functionality of the proposed control method.

Publication VII

The paper proposes a hybrid observer for sensorless control of permanent magnet synchronous motor drives equipped with an inverter output LC filter. An adaptive full-order observer is augmented with a high-frequency signal injection method at low speeds. The only measured quantities are the inverter phase currents and the dc-link voltage. The effects of the LC filter on the signal injection are investigated, and it is shown that the filter is not an obstacle to using signal injection methods. The proposed method allows sensorless operation in a wide speed range down to zero speed. Experimental results are given to confirm the effectiveness of the proposed method.

Publication VIII

The paper proposes a motion-sensorless control method for permanent magnet synchronous motor drives when only the DC-link current is measured instead of the motor phase currents. A two-phase pulse-width modulation method is used, allowing the DC-link current to be sampled twice in a switching period at uniform intervals during active voltage vectors. A method is proposed for obtaining the current feedback for vector control, and an adaptive observer is used for estimating the rotor speed and position. The estimation is augmented with a high-frequency signal injection method at low speeds; a modified high-frequency excitation voltage is proposed for better performance. The proposed method enables stable operation of the permanent magnet synchronous motor drive in a wide speed range and under various loads. The effectiveness of the proposed method is demonstrated both by simulations and laboratory experiments.

Publication IX

The paper proposes an on-line method for the estimation of the stator resistance and the permanent magnet flux in sensorless permanent magnet synchronous motor drives. An adaptive observer augmented with a high-frequency signal injection technique is used for sensorless control. The observer contains excess information that is not used for the speed and position estimation. This information is used for the adaptation of the motor parameters: at low speeds, the stator resistance is estimated, whereas at medium and high speeds, the permanent magnet flux is estimated. Small-signal analysis is carried out to investigate the proposed method. The convergence of the parameter estimates is shown by simulations and laboratory experiments. The stator resistance adaptation works down to zero speed in sensorless control.

5.2 Contribution of the Thesis

The main scientific contributions of this thesis are as follows:

- A modified voltage model and an adaptive observer are augmented with a high-frequency signal injection method such that the transition between low and medium speeds is smooth and the dynamics of the fundamental-excitation method are maintained at low speeds
- The dynamic properties of the adaptive observer are investigated for salient-rotor PMSMs, and a feedback gain is proposed to improve the dynamic properties

- Signal injection is used for the stator resistance adaptation at low speeds simultaneously with the rotor position estimation. The estimated stator resistance is adjusted such that the correction term of the signal injection method is driven to zero.
- It is shown that spatial harmonics in the PMSM result in speed and position estimation errors. The errors are compensated by taking the harmonics into account in the adaptive observer and by modifying the excitation voltage of the high-frequency signal injection method.
- The torque ripple is suppressed in sensorless salient-rotor PMSM drives in such a way that the reluctance torque is used, and in addition to the flux harmonics, the inductance harmonics are taken into account
- High-frequency signal injection is used without additional measurements in a sensorless PMSM drive equipped with an inverter output filter
- An adaptive observer combined with a high-frequency signal injection method is developed for a system equipped with inverter DC-link current measurement

Chapter 6

Conclusions

Control methods for motion-sensorless PMSM drives were investigated in this thesis. For the speed and position estimation, both fundamental-excitation methods and signal injection methods were studied. Two different hybrid methods were proposed, where a modified voltage model and an adaptive observer are combined with a high-frequency signal injection method. The latter is the basis of most of the methods proposed in this thesis. All the methods are investigated both by simulations and laboratory experiments.

The novelty of the hybrid methods proposed in the thesis is that the effect of the fundamental-excitation method on the estimation is not reduced at low speeds. Hence, good dynamic properties are maintained although the signal injection method dominates the estimation in steady state. The dynamic properties of the adaptive observer were investigated, and a feedback gain was proposed to improve the estimation dynamics. For reducing the parameter sensitivity of the adaptive observer, a method was developed for the adaptation of the stator resistance and the permanent magnet flux. The parameter adaptation exploits information in the observer that is not used for sensorless control.

Spatial harmonics in the permanent magnet flux and in the stator inductance are included in the PMSM model. The harmonics are included in the adaptive observer, and the HF excitation voltage of the signal injection method is modified for reduction of the effects of the inductance harmonics on the position estimation at low speeds. As a result, the estimation accuracy of the combined observer is improved. For the reduction of torque ripple, a new scheme was developed where the harmonics in the torque are estimated and controlled to zero. The method is simple due to the absence of look-up tables, it takes inductance harmonics into account in addition to the flux harmonics, it has a good torque-to-current ratio because reluctance torque is used, and it is suitable for sensorless drives.

The signal injection was investigated in drives equipped with an LC filter at the inverter output and in drives equipped with inverter DC-link current measurement. In both cases, the signal injection was found suitable for the position estimation at low speeds. With the DC-link current measurement, the high-frequency current feedback is based partly on the estimated stator current provided by the adaptive observer. Hence, the system can cope with irregularly obtained current samples.

In commercial PMSMs, the saturation cannot be omitted if good estimation and control accuracy is required. Therefore, suitable future research topics include modeling and identification of the magnetic saturation. In addition, the initial position of the rotor has to be identified before normal operation. Identification of the electrical parameters of the PMSM, including the spatial harmonics, is also essential since the parameters are rarely known in practice.

Bibliography

Aihara, T., Toba, A., Yanase, T., Mashimo, A., and Endo, K. (1999). "Sensorless torque control of salient-pole synchronous motor at zero-speed operation." *IEEE Trans. Ind. Electron.*, **14**(1), pp. 202–208.

Andreescu, G. D. (1999). "Position and speed sensorless control of PMSM drives based on adaptive observer." In *Proc. EPE'99*, Lausanne, Switzerland, CD-ROM.

Batzel, T. D. and Lee, K. Y. (2005). "Electric propulsion with sensorless permanent magnet synchronous motor: implementation and performance." *IEEE Trans. Energy Convers.*, **20**(3), pp. 575–583.

Bianchi, N. and Bolognani, S. (1998). "Magnetic models of saturated interior permanent magnet motors based on finite element analysis." In *Conf. Rec. IEEE-IAS Annu. Meeting*, p. 27–34, St. Louis, MO.

Bianchi, N., Bolognani, S., Jang, J.-H., and Sul, S.-K. (2007). "Comparison of PM motor structures and sensorless control techniques for zero-speed rotor position detection." *IEEE Trans. Pow. Electron.*, **22**(6), pp. 2466–2475.

Blaabjerg, F., Pedersen, J. K., Jaeger, U., and Thoegersen, P. (1997). "Single current sensor technique in the DC link of three-phase PWM-VS inverters: a review and a novel solution." *IEEE Trans. Ind. Applicat.*, **33**(5), pp. 1241–1253.

Blaschke, F. (1972). "The principle of field orientation applied to the new transvector closed-loop control system for rotating field machines." *Siemens-Rev.*, **39**, pp. 217–220.

Boldea, I. and Nasar, S. A. (1988). "A general equivalent circuit (gec) of electric machines including crosscoupling saturation and frequency effects." *IEEE Trans. Energy Convers.*, **3**(3), pp. 689–695.

Bolognani, S., Oboe, R., and Zigliotto, M. (1999). "Sensorless full-digital PMSM drive with EKF estimation of speed and rotor position." *IEEE Trans. Ind. Electron.*, **46**(1), pp. 184–191.

Briz del Blanco, F., Degner, M. W., and Lorenz, R. D. (1999). "Dynamic analysis of current regulators for AC motors using complex vectors." *IEEE Trans. Ind. Applicat.*, **35**(6), pp. 1424–1432.

Carpita, M., Colombo, D., Monti, A., and Fradilli, A. (1991). "Power converter filtering techniques design for very high speed drive systems." In *Proc. EPE'01*, Graz, Austria.

Chen, Z., Tomita, M., Doki, S., and Okuma, S. (2003). "An extended electromotive force model for sensorless control of interior permanent-magnet synchronous motors." *IEEE Trans. Ind. Electron.*, **50**(2), pp. 288–295.

Choi, J. W. and Sul, S.-K. (1995). "A new compensation strategy reducing voltage/current distortion in PWM VSI systems operating with low output voltages." *IEEE Trans. Ind. Applicat.*, **31**(5), pp. 1001–1008.

Chung, S., Kim, H., Kim, C., and Youn, M. (1998). "A new instantaneous torque control of PM synchronous motor for high performance direct drive applications." *IEEE Trans. Pow. Electron.*, **13**(3), pp. 388–400.

Colamartino, F., Marchand, C., and Razek, A. (1999). "Torque ripple minimization in permanent magnet synchronous servodrive." *IEEE Trans. Energy Convers.*, **14**(3), pp. 616–621.

Consoli, A., Musumeci, S., Raciti, A., and Testa, A. (1994). "Sensorless vector and speed control of brushless motor drives." *IEEE Trans. Ind. Electron.*, **41**(1), pp. 91–96.

Consoli, A., Scarcella, G., and Testa, A. (2001). "Industry application of zero-speed sensorless control techniques for PM synchronous motors." *IEEE Trans. Ind. Applicat.*, **37**(2), pp. 513–521.

Corley, M. and Lorenz, R. D. (1998). "Rotor position and velocity estimation for a salient-pole permanent magnet synchronous machine at standstill and high speeds." *IEEE Trans. Ind. Applicat.*, **43**(4), pp. 784–789.

De Angelo, C., Bossio, G., Solsona, J., Garćia, G. O., and Valla, M. I. (2005). "A rotor position and speed observer for permanent-magnet motors with nonsinusoidal EMF waveform." *IEEE Trans. Ind. Electron.*, **52**(3), pp. 807–813.

de Jong, H. (1980). "Saturation in electrical machines." In *Proc. ICEM/1980*, vol. 3, pp. 1545–1552, Athens, Greece.

Degner, M. W. and Lorenz, R. D. (1998). "Using multiple saliencies for the estimation of flux, position, and velocity in AC machines." *IEEE Trans. Ind. Applicat.*, **34**(5), pp. 1097–1104.

Depenbrock, M. (1988). "Direct self-control (DSC) of inverter-fed induction machine." *IEEE Trans. Pow. Electron.*, **3**(4), pp. 420–429.

Dhaouadi, R., Mohan, N., and Norum, L. (1991). "Design and implementation of an extended kalman filter for the state estimation of a permanent magnet synchronous motor." *IEEE Trans. Pow. Electron.*, **6**(3), pp. 491–497.

Ertugrul, N. and Acarnley, P. (1994). "A new algorithm for sensorless operation of permanent magnet motors." *IEEE Trans. Ind. Applicat.*, **30**(1), pp. 126–133.

Eskola, M. (2006). *Speed and Position Sensorless Control of Permanent Magnet Synchronous Motors in Matrix Converter and Voltage Source Converter Applications*. D.Tech. thesis, Tampere University of Technology, Tampere, Finland.

Furuhashi, T., Sangwongwanich, S., and Okuma, S. (1992). "A position-and-velocity sensorless control for brushless DC motors using an adaptive sliding mode observer." *IEEE Trans. Ind. Electron.*, **39**(2), pp. 89–95.

Green, T. C. and Williams, B. W. (1989). "Derivation of motor line-current waveforms from the DC-link current of an inverter." *Proc. Inst. Elect. Eng. B*, **136**(4), pp. 196–204.

Guerrero, J. M., Leetmaa, M., Briz, F., Zamarrón, A., and Lorenz, R. D. (2005). "Inverter nonlinearity effects in high-frequency signal-injection-based sensorless control methods." *IEEE Trans. Ind. Applicat.*, **41**(2), pp. 618–626.

Ha, J. I., Ide, K., Sawa, T., and Sul, S. K. (2003). "Sensorless rotor position estimation of an interior permanent-magnet motor from initial states." *IEEE Trans. Ind. Applicat.*, **39**(3), pp. 761–767.

Ha, J. I. and Sul, S. K. (1999). "Sensorless field-orientation control of an induction machine by high-frequency signal injection." *IEEE Trans. Ind. Applicat.*, **35**(1), pp. 45–51.

Habetler, T. and Divan, D. M. (1991). "Control strategies for direct torque control using discrete pulse modulation." *IEEE Trans. Ind. Applicat.*, **27**(5), pp. 893–901.

Harnefors, L. and Nee, H.-P. (2000). "A general algorithm for speed and position estimation of AC motors." *IEEE Trans. Ind. Electron.*, **47**(1), pp. 77–83.

Ichikawa, S., Tomita, M., Doki, S., and Okuma, S. (2006). "Sensorless control of permanent-magnet synchronous motors using online parameter identification based on system identification theory." *IEEE Trans. Ind. Electron.*, **53**(2), pp. 363–372.

Ide, K., Ha, J.-I., Sawamura, M., Iura, H., and Yamamoto, Y. (2002). "A novel hybrid speed estimator of flux observer for induction motor drives." In *Proc. IEEE ISIE'02*, vol. 3, pp. 822–827, L'Aquila, Italy.

Jahns, T., Kliman, G., and Neumann, T. (1986). "Interior permanent-magnet synchronous motors for adjustable-speed drives." *IEEE Trans. Ind. Applicat.*, **22**(4), pp. 738–747.

Jang, J.-H., Sul, S.-K., Ha, J.-I., Ide, K., and Sawamura, M. (2003). "Sensorless drive of surface-mounted permanent-magnet motor by high-frequency signal injection based on magnetic saliency." *IEEE Trans. Ind. Applicat.*, **39**(4), pp. 1031– 1039.

Jansen, P. L. and Lorenz, R. D. (1995). "Transducerless position and velocity estimation in induction and salient AC machines." *IEEE Trans. Ind. Applicat.*, **31**(2), pp. 240–247.

Jansen, P. L. and Lorenz, R. D. (1996). "Transducerless field orientation concepts employing saturation-induced saliencies in induction machines." *IEEE Trans. Ind. Applicat.*, **32**(6), pp. 1380–1393.

Jeong, S.-G. and Park, M.-H. (1991). "The analysis and compensation of dead-time effects in PWM inverters." *IEEE Trans. Ind. Electron.*, **38**(2), pp. 108–114.

Jones, L. A. and Lang, J. H. (1989). "A state observer for permanent-magnet synchronous motor." *IEEE Trans. Ind. Electron.*, **36**(3), pp. 374–382.

Kim, H. and Jahns, T. M. (2006). "Phase current reconstruction for AC motor drives using a DC link single current sensor and measurement voltage vectors." *IEEE Trans. Pow. Electron.*, **21**(5), pp. 1413–1419.

Kim, J. and Sul, S. (1995). "High performance PMSM drives without rotational position sensors using reduced order observer." In *Conf. Rec. IEEE-IAS Annu. Meeting*, vol. 1, pp. 75–82, Orlando, FL.

Kim, K.-H., Chung, S.-K., Moon, G.-W., Baik, I.-C., and Youn, M.-J. (1995). "Parameter estimation and control for permanent magnet synchronous motor drive using model reference adaptive technique." In *Proc. IEEE IECON'95*, vol. 1, pp. 387–392, Orlando, FL.

Kobayashi, T., Kubota, H., and Nakagawa, S. (2006). "Investigation of ipmsm's position estimation method in very low speed region with DC link current detection." In *Proc. IEEE IECON'06*, pp. 885–890, Paris, France.

Koonlaboon, S. and Sangwongwanich, S. (2005). "Sensorless control of interior permanent-magnet synchronous motors based on a fictitious permanent-magnet flux model." In *Conf. Rec. IEEE-IAS Annu. Meeting*, vol. 1, pp. 311–318, Hong Kong.

Krause, P. C., Wasynczuk, O., and Sudhoff, S. D. (2002). *Analysis of Electric Machinery and Drive Systems*. IEEE Press, Piscataway, NJ.

Kubota, H., Matsuse, K., and Nakano, T. (1993). "DSP-based speed adaptive flux observer of induction motor." *IEEE Trans. Ind. Applicat.*, **29**(2), pp. 344–348.

Kulkarni, A. B. and Ehsani, M. (1992). "A novel position sensor elimination technique for the interior permanent-magnet synchronous motor drive." *IEEE Trans. Ind. Applicat.*, **28**(1), pp. 144–150.

Lagerquist, R., Boldea, I., and Miller, T. J. (1994). "Sensorless control of the synchronous reluctance motor." *IEEE Trans. Ind. Applicat.*, **30**(3), pp. 673–682.

Li, Y., Zhu, Z. Q., Howe, D., Bingham, C. M., and Stone, D. (2007). "Improved rotor position estimation by signal injection in brushless AC motors, accounting for cross-coupling magnetic saturation." In *Conf. Rec. IEEE-IAS Annu. Meeting*, New Orleans, LA.

Linke, M., Kennel, R., and Holtz, J. (2002). "Sensorless position control of permanent magnet synchronous machines without limitation at zero speed." In *Proc. IEEE IECON'02*, vol. 1, pp. 674–679, Sevilla, Spain.

Low, T. S., Tseng, K. J., Lee, T. H., Lim, K. W., and Lock, K. S. (1990). "Strategy for the instantaneous torque control of permanent-magnet brushless DC drives." *IEE Proc. B, Elect. Power Appl.*, **137**(6), pp. 355–363.

Madani, A., Barbot, J., Colamartino, F., and Marchand, C. (1995). "Reduction of torque pulsations by inductance harmonics identification of a permanent-magnet synchronous machine." In *Proc. IEEE CCA'95*, pp. 787–792, Albany, NY.

Melkebeek, J. A. and Willems, J. L. (1990). "Reciprocity relations for the mutual inductances between orthogonal axis windings in saturated salient-pole machines." *IEEE Trans. Ind. Applicat.*, **26**(1), pp. 107–114.

Morimoto, S., Kawamoto, K., Sanada, M., and Takeda, Y. (2002). "Sensorless control strategy for salient-pole PMSM based on extended EMF in rotating reference frame." *IEEE Trans. Ind. Applicat.*, **38**(4), pp. 1054–1061.

Moynihan, J. F., Bolognani, S., Kavanagh, R. C., Egan, M. G., and Murphy, J. M. D. (1993). "Single sensor current control of ac servodrives using digital signal processors." In *Proc. EPE'93*, vol. 4, pp. 415–421, Brighton, UK.

Ohtani, T., Takada, N., and Tanaka, K. (1992). "Vector control of induction motor without shaft encoder." *IEEE Trans. Ind. Applicat.*, **28**(1), pp. 157–164.

Parasiliti, F., Petrella, R., and Tursini, M. (2002). "Sensorless speed control of salient rotor PM synchronous motor based on high frequency signal injection and kalman filter." In *Proc. IEEE ISIE'02*, vol. 2, pp. 623–628, L'Aquila, Italy.

Park, M.-H. and Lee, H.-H. (1989). "Sensorless vector control of permanent magnet synchronous motor using adaptive identification." In *Proc. IEEE IECON'89*, vol. 1, pp. 209–214, Philadelphia, PA.

Pedersen, J. K., Blaabjerg, F., Jensen, J. W., and Thogersen, P. (1993). "An ideal PWM-VSI inverter with feedforward and feedback compensation." In *Proc. EPE'93*, vol. 5, pp. 501–507, Brighton, UK.

Piippo, A., Hinkkanen, M., and Luomi, J. (2005). "Analysis of an adaptive observer for sensorless control of PMSM drives." In *Proc. IEEE IECON'05*, pp. 1474–1479, Raleigh, NC.

Piippo, A., Hinkkanen, M., and Luomi, J. (2007a). "Adaptation of motor parameters in sensorless PMSM drives." In *Proc. PEDS 2007*, pp. 175–182, Bangkok, Thailand.

Piippo, A., Salomäki, J., and Luomi, J. (2007b). "Signal injection in sensorless PMSM drives equipped with inverter output filter." In *Proc. PCC-Nagoya 2007*, pp. 1105–1110, Nagoya, Japan.

Salomäki, J., Hinkkanen, M., and Luomi, J. (2006). "Sensorless control of induction motor drives equipped with inverter output filter." *IEEE Trans. Ind. Electron.*, **53**(4).

Sattler, P. K. and Stärker, K. (1989). "Estimation of speed and pole position of an inverter fed permanent excited synchronous machine." In *Proc. EPE'89*, vol. 3, pp. 1207–1212, Aachen, Germany.

Schmirgel, H. and Krah, J. O. (2005). "Compensation of nonlinearities in the IGBT power stage of servo amplifiers through feed forward control in the current loop." In *Proc. PCIM Europe 2005*, pp. 94–99, Nuremberg, Germany.

Schroedl, M. (1988). "Detection of the rotor position of a permanent magnet synchronous machine at standstill." In *Proc. ICEM/1988*, pp. 195–197, Pisa, Italy.

Schroedl, M. (1996). "Sensorless control of AC machines at low speed and standstill based on the "INFORM" method." In *Conf. Rec. IEEE-IAS Annu. Meeting*, vol. 1, pp. 270–277, San Diego, CA.

Shin, M., Hyun, D., Cho, S., and Choe, S. (2000). "An improved stator flux estimation for speed sensorless stator flux orientation control of induction motors." *IEEE Trans. Pow. Electron.*, **15**(2), pp. 312–318.

Silva, C., Asher, G. M., and Sumner, M. (2003). "An hf signal-injection based observer for wide speed range sensorless PM motor drives including zero speed." In *Proc. EPE'03*, vol. 1, pp. 1–9, Toulouse, France.

Song, H. and Nam, K. (1999). "Dual current control scheme for PWM converter under unbalanced input voltage conditions." *IEEE Trans. Ind. Electron.*, **46**(5), pp. 953–959.

Springob, L. and Holtz, J. (1998). "High-bandwidth current control for torque-ripple compensation in PM synchronous machines." *IEEE Trans. Ind. Electron.*, **45**(5), pp. 713–721.

Stumberger, G., Stumberger, B., and Dolinar, D. (2003). "Evaluation of saturation and cross-magnetization effects in interior permanent-magnet synchronous motor." *IEEE Trans. Ind. Applicat.*, **39**(5), pp. 1264–1271.

Takahashi, I. and Noguchi, T. (1986). "A new quick-response and high-efficiency control strategy of an induction motor." *IEEE Trans. Ind. Applicat.*, **IA-22**(5), pp. 820–827.

Teodorescu, R., Bech, M., Blaabjerg, F., and Pedersen, J. (2000). "Flexible drive systems laboratory – a modern teaching facility in electrical drives at aalborg university." In *Proc. NORPIE/2000*, pp. 42–46, Aalborg, Denmark.

Teske, N., Asher, G. M., Sumner, M., and Bradley, K. J. (2000). "Suppression of saturation saliency effects for the sensorless position control of induction motor drives under loaded conditions." *IEEE Trans. Ind. Electron.*, **47**(5), pp. 1142–1150.

Tursini, M., Petrella, R., and Parasiliti, F. (2003a). "Initial rotor position estimation method for PM motors." *IEEE Trans. Ind. Applicat.*, **39**(6), pp. 1630–1640.

Tursini, M., Petrella, R., and Parasiliti, F. (2003b). "Sensorless control of an IPM synchronous motor for city-scooter applications." In *Conf. Rec. IEEE-IAS Annu. Meeting*, vol. 3, pp. 1472–1479, Salt Lake City, UT.

Urasaki, N., Kinjo, T. S. T., Funabashi, T., and Sekine, H. (2005). "Dead-time compensation strategy for permanent magnet synchronous motor drive taking zero-current clamp and parasitic capacitance effects into account." *IEE Proc. Electr. Power Appl.*, **152**(4), pp. 845–853.

Vas, P., Hallenius, K. E., and Brown, J. E. (1986). "Cross-saturation in smooth-air-gap electrical machines." *IEEE Trans. Energy Convers.*, **EC-1**(1), pp. 103–109.

Wallmark, O. and Harnefors, L. (2006). "Sensorless control of salient PMSM drives in the transition region." *IEEE Trans. Ind. Electron.*, **53**(4), pp. 1179–1187.

Wu, A. P. and Chapman, P. L. (2005). "Simple expressions for optimal current waveforms for permanent-magnet synchronous machine drives." *IEEE Trans. Energy Convers.*, **20**(1), pp. 151–157.

Wu, R. and Slemon, G. R. (1991). "A permanent magnet motor drive without a shaft sensor." *IEEE Trans. Ind. Applicat.*, **27**(5), pp. 1005–1011.

Xie, G. and Ramshaw, R. S. (1986). "Nonlinear model of synchronous machines with saliency." *IEEE Trans. Energy Convers.*, **EC-1**(3), pp. 198–204.

Xu, X. and Novotny, D. W. (1991). "Implementation of direct stator flux orientation control on a versatile DSP based system." *IEEJ Trans. Ind. Applicat.*, **27**(4), pp. 694–700.

Yang, G., Tomioka, R., Nakano, M., and Chin, T. H. (1993). "Position and speed sensorless control of brushless DC motor based on an adaptive observer." *IEEJ Trans. Ind. Applicat.*, **113**, pp. 579–586.

Yong, S.-I., Choi, J.-W., and Sul, S.-K. (1994). "Sensorless vector control of induction machine using high frequency current injection." In *Conf. Rec. IEEE-IAS Annu. Meeting*, vol. 1, pp. 503–508, Denver, CO.

Zimmermann, W. (1988). "Feldorientiert geregelter Umrichterantrieb mit sinusförmigen Maschinenspannungen." *etzArchiv*, **10**(8), pp. 259–266.

ISBN 978-951-22-9378-0
ISBN 978-951-22-9379-7 (PDF)
ISSN 1795-2239
ISSN 1795-4584 (PDF)